LASER DRILLING OF METALS AND GLASS USING ZERO-ORDER BESSEL BEAMS

Humbelani Edzani Ratsibi

Thesis presented in fulfilment of the requirements for the degree of Magister Scientiae at the University of the Western Cape

UNIVERSITY of the
WESTERN CAPE

Supervisor: Dr. S. Halindintwali, University of the Western Cape

Co-supervisors: Mr H. P. Burger, CSIR-National Laser Center

Prof. A. Forbes, CSIR-National Laser Center

December 2013

DECLARATION

I declare that *LASER DRILLING OF METALS AND GLASS USING ZERO-ORDER BESSEL BEAMS* is my own original work, that I have not previously in its entirety or in part submitted it to any university for a degree and that all sources I have used or quoted have been indicated and acknowledged by complete references.

Humbelani Edzani Ratsibi

UNIVERSITY of the
WESTERN CAPE

17 December 2013

Signature:…… ……

To:

My parents

Mphaya and Avhashoni

Ratsibi

UNIVERSITY of the
WESTERN CAPE

In memory of my late grandmother Vho-Muofhe Mbuleni Lukoto!

Acknowledgements

Firstly I would like to thank God the almighty for giving me the wisdom, strength and ability to study till this far. I would love to thank my mom and dad for their enormous support throughout my studies, my dad taking pride in my achievements and my mom constantly on her knees praying for my success. To my siblings Vusani and Lindelani thank you for being the older supportive brother and sister. To my nephew Mulondo thank you for the laughter filled moments with you and your unending questions and stories, that kept me sane throughout my studies.

To my friends and colleagues I want to thank you all for the support, and lending me your ears when I had to pour out my frustrations and bouncing ideas. To Mr Johan Steyn and Dr Saturnin Ombinda thank you for always willing to help with the laser even when you didn't have to go all out, you did so in a helpful manner.

To my mentor and friend Dr Tleyane Sono I would like to express my sincere gratitude for all your help in this project. Thank you for taking the time to read my work and all your advices and inputs.

I would also like to thank the staff at the NLC-LMP for the willingness to assist in every way possible. To my Supervisors Prof. Andrew Forbes, Mr Herman Burger, and Dr Sylvain Halinndintwali thank you for your patience in this project and the encouragement you never stopped giving me.

To everyone who has been a part of this journey I would like to express my greatest and humble gratitude.

Khomba ya ha Ratsibi, lupedzi lwa Mphaya luri ani ntshileli.

Aaa!

UNIVERSITY of the
WESTERN CAPE

Abstract

This dissertation consists of two main sections. The first section focuses on generating zero order Bessel beams using axicons. An axicon with an opening angle $\gamma = 5°$ was illuminated with a Gaussian beam of width $\omega_0 = 1.67$ mm from a cw fiber laser with central wavelength $\lambda = 1064$ nm to generate zero order Bessel beams with a central spot radius $r_0 = 8.3 \pm 0.3$ µm and propagation distance $\frac{1}{2}z_{max} = 20.1 \pm 0.5$ mm. The central spot size of a Bessel beam changes slightly along the propagation distance. The central spot radius r_0 can be varied by changing the opening angle of the axicon, γ, and the wavelength of the beam. The second section focuses on applications of the generated Bessel beams in laser microdrilling. A Ti:Sapphire pulsed femtosecond laser ($\lambda = 775$ nm, $\omega_0 = 2.55$ mm, repetition rate 1 kHz, pulse energy 1 mJ, and pulse duration 150 fs) was used to generate the Bessel beams for drilling stainless steel thin sheets of thickness 50 µm and 100 µm and microscopic glass slides 1 mm thick. The central spot radius was $r_0 = 15.9 \pm 0.3$ µm and $\frac{1}{2}z_{max} = 65.0 \pm 0.5$ mm. The effect of the Bessel beam shape on the quality of the holes was analysed and the results were discussed. It was observed that Bessel beams drill holes of better quality on transparent microscopic glass slides than on stainless steel sheet. The holes drilled on stainless steel sheets deviated from being circular on both the top and bottom surface for both thicknesses. However the holes maintained the same shape on both sides of each sample, indicating that the walls are close to being parallel. The holes drilled on the glass slides were circular and their diameters could be measured. The measured diameter (15.4 ± 0.3 µm) of the hole is smaller than the diameter of the central spot (28.2 ± 0.1 µm) of the Bessel beam. Increasing the pulse energy increased the diameter of the drilled hole to a value close to the measured diameter of the central spot.

UNIVERSITY of the
WESTERN CAPE

Contents

Declaration

Acknowledgements

Abstract

Chapter 1: Introduction

1.1 Overview of laser drilling 1

1.2 Beam Shaping in Laser Drilling 2

1.2.1 Bessel beams 3

1.3 Aim and outline of this thesis 4

Chapter 2: Laser beam shaping

2.1 Introduction 5

2.2 Gaussian Beams 5

2.2.1 Propagation Parameters 8

2.2.1.1 Beam width 8

2.2.1.2 Divergence 9

2.2.1.3 Radius of Curvature 9

2.3 Bessel Beams 10

2.3.1 Generation of Bessel Beams using axicons 14

2.4. Experimental procedure for generation and characterisation of Bessel and annular beams 20

2.4.1 Experimental setup using an axicon 21

2.4.2 Magnification system 22

2.4.3 Experimental setup for generating an annular beam. 23

2.5 Results and discussion 24

2.6 Conclusion 37

Chapter 3: Laser drilling

3.1 Introduction 38

3.1.1 Laser drilling techniques 39

3.1.2 Defects associated with laser drilling 42

UNIVERSITY of the
WESTERN CAPE

3.1.3 Laser Parameters that affect laser hole drilling process 43
3.1.3.1 Pulse energy 43
3.1.3.2 Peak power 43
3.1.3.3 Number of pulses 44
3.1.3.4 Pulse duration and frequency 45
3.1.3.5 Focusing conditions 45
3.1.3.6 Assist gas 46
3.2 Ultra-short pulsed lasers 46
3.3 Applications of Bessel beams in micro-drilling 47
3.3.1 Literature review 47
3.3.2 Experimental procedure 50
3.4 Characterisation techniques 52
3.4.1 Optical Microscopy 53
3.4.2 Scanning Electron Microscopy 55
3.4.2.1 Introduction 55
3.4.2.2 Electron Beam-Specimen Interaction 56
3.4.2.3 Resolution 58
3.4.2.4 Depth of Field and Working Distance 59
3.4.2.5 Effect of accelerating voltage 60
3.4.2.6 Sample preparation 60
3.4.3 Characterisation 61
3.4.3.1 Optical Microscopy Instrumentation 61
3.4.3.2 Scanning Electron Microscopy Instrumentation 61

Chapter 4: Results and discussions

4.1 Experimental results and discussions 62
4.1.1 Bessel beam generation 62
4.1.2 Laser drilling results and discussions 64
4.2 Conclusion 83
Summary 84
Future work 85
References 86

UNIVERSITY of the
WESTERN CAPE

Chapter 1
Introduction

1.1 Overview on laser drilling

Application of laser micromachining technology has grown rapidly over the last decade particularly in material processing for scientific and industrial applications. One of the major reasons for the interest into this field has been the ability of lasers to offer a highly directional and localized source which facilitates material modifications at precise locations with minimum damage on the surroundings [1]. It is challenging to use conventional machining methods such as mechanical drilling in making 3D structures when micron-sized processing is required. This is mainly because the wear and elastic deformation of processing tools caused by the contact with the working materials cannot be disregarded [1]. Beam processing became the advanced technology for 3-dimensional microstructure micromachining. Laser beam machining is able to improve on the limitations caused by traditional machining technology as it is a precise, fast, and a contactless technology [1-5].

Laser drilling is one of the micromachining processes that has become very popular in industries such as medical engineering e.g. producing suture holes on surgical needles and meshes; automobile manufacturing, for drilling holes on stainless steel fuel filters; and in aviation, for drilling holes in the outer skin of the tail fin to reduce air vortices and air resistance [3]. It is a noncontact, precise, and reproducible technique that is used to form small diameter (≤ 100 μm) and high aspect ratio holes in a wide range of materials [5]. It is considered as an alternative for drilling techniques such as mechanical drilling, electro discharge machining, electrochemical machining, and electron beam drilling [3]. Laser drilling has the ability to drill holes in difficult-to-machine materials such superalloys, ceramics, and composites without tool wear rate [5].

For drilling to take place, a high intensity beam is focused onto the surface at high power densities generally above10^7 W/cm^2 [4], sufficient to heat, melt and subsequently eject the material in both liquid and vapour phases. Drilling is mostly carried out with a pulsed laser, where the pulse duration is much shorter than the thermal response time of the material. A coaxial assist gas is often used while drilling in order to shield the laser optics from contamination from the ejected debris and also to facilitate the material removal [4-5].

In the aerospace industry the geometric and metallurgical aspects of the drilled holes are very critical. Laser drilling process is often associated with defects such as taper, circularity, spatter, heat-affected zone, recast layer and microcracking. For most applications, parallel-sided holes with minimum taper, resolidification and surface debris are required. Bandyopadhyay et al. [6] listed laser parameters that are vital for laser drilling as the beam energy, spot size, beam shape, wavelength, fluence, polarization and, in the case of pulsed lasers, pulse duration and repetition rate [6].

UNIVERSITY of the
WESTERN CAPE

1.2 Beam Shaping in Laser Drilling

Laser beam shaping is essential in optimizing a large number of laser material processing applications, laser drilling being one of them. A beam shape can be defined as a spatial intensity distribution. Optical elements are used to transform the conventional circular Gaussian beam into the desired shape. Some of the desired shapes used in laser drilling include flat-top beams [7, 8], Bessel beams [1, 2], and annular beams [8]. In this dissertation a refractive axicon is used to transform Gaussian beams into Bessel beams and annular beams.

Work has been done in determining the effect that the beam shape has on the quality of the drilled holes. The quality of the drilled hole is quantified by the entrance and exit diameter, taper angle, and the aspect ratio between the width of the hole and the thickness of the material. Gaussian beams can focus to a tight micron-sized

spot over a short focal range. Due to the short focal range the drilled holes typically have a taper. Some applications require taper free holes, although this is difficult to achieve. Alternative ways to reduce taper angles in drilled holes were studied. Matsuoka et al. [1] used Bessel beams to drill through holes with a diameter less than 10 μm on a stainless steel sheet 20 μm thick. They showed that the taper of the hole drilled with a Bessel beam is smaller than that drilled with a Gaussian beam [1].

1.2.1 Bessel beams

Bessel beams are defined as “non-diffracting” beams since they are not subject to transverse spreading. They were first discovered by Durnin as exact solutions to the free-space Helmholtz’s wave equation, described by Bessel functions [9, 10]. An ideal Bessel beam contains an infinite number of rings over an infinite area thus carrying infinite energy. A thorough description of Bessel beams is given in detail in chapter 2.

Bessel beams were chosen mainly due to their special properties, e.g. they possess a micron-sized focal spot over a long focal range [1] and can reconstruct after an obstacle [11]. They offer the ability to drill micron-sized holes on structured, rough, or uneven samples, or non-planer samples, because they can combine a narrow central lobe with a long focal range [7].

However two major disadvantages were noted for laser drilling using Bessel beams. The first being the visible ring structure on the top surface of the irradiated material [7]. The ring structure is caused by the energy in the surrounding rings of the Bessel beam, since the energy is distributed evenly amongst the rings and only the intensity differs amongst the rings. Kohno and Matsuoka [2] resolved this problem by controlling the beam energy strength of the main lobe of the Bessel beam just to be above the ablation threshold [2]. Another alternative solution is to generate Bessel beams with fewer rings using spatial light modulators.

The second disadvantage lies in the limitation of drilling metals with Bessel beams since they are opaque. Bessel beams are considered to be a result of the

interference between plane waves. They are known to reconstruct after encountering an obstacle [11]. In the case of metals, due to they are opacity, such plane waves do not propagate inside the material, and thus the long depth of field of the Bessel beam would be lost. However drilling of very thin metal foils (100 μm or less) using Bessel beams have resulted in sharper sidewall and less taper than holes drilled with Gaussian beams on the same sample. Kohno and Matsuoka [2] drilled an almost straight hole with a high aspect ratio (about 20) on stainless steel (SUS304) plate 100-μm-thick.

1.3 Aim and outline of this thesis

The aim of this thesis is to drill good quality circular holes with minimal taper on metals using Bessel beams with minimal surrounding rings. Micron-sized holes have been drilled on very thin stainless steel sheets without eliminating the effect of the external ring structure on the top surface of the sheets [2]. With the suggested ways to resolve the problem of external ring structure, we want to improve from the current state of the quality of drilled holes on stainless steel sheets using Bessel beams.

UNIVERSITY of the
WESTERN CAPE

In chapter 2 we give an overview on beam shaping, and an in-depth study of the properties of Bessel beams is conducted together with ways of generating these beams. Axicons will be used for the generation of Bessel beams. The properties of these beams will be measured and results will be discussed.

Chapter 3 will give a comprehensive background on laser drilling process, its techniques, processing parameters and defects arising from the process. Furthermore generated Bessel beams will be used to drill holes on the specified materials. The characterization techniques used will be thoroughly discussed in this chapter.

The drilled holes will be analysed and the results will be discussed in chapter 4. At the end of this chapter a summary of the dissertation will be given and possible aspects of future work will be suggested.

Chapter 2
Laser Beam Shaping

2.1 Introduction

Laser machining has become widely used and is an established method for the fast and efficient processing of a variety of materials. Various parameters such as wavelength, beam shape, beam form (continuous wave (cw) or pulsed), power density and beam quality (M^2) play a vital role in laser material processing. Beam shaping is defined as the art of controlling the irradiance and phase profile of the output of a laser [12]. The shape of the beam is associated with the irradiance profile, while propagation properties of the irradiance distribution are governed by phase profiles.

Most lasers operate in the fundamental transverse electromagnetic mode of a cavity providing a Gaussian intensity profile. However it is possible to change the shape of the beam for example by propagating it through beam shaping optical systems. The characteristics of beam shaping are discussed in the following sub-sections, a distinction is made between the Gaussian and Bessel beam shapes.

UNIVERSITY of the
WESTERN CAPE

2.2 Gaussian Beams

Gaussian light beams are those whose transverse electric field and intensity distributions are approximated by a Gaussian function. They remain Gaussian even after passing through simple optical elements such as lenses. Because of this property, Gaussian beams are favourable in many applications [12].

Gaussian beams have a Gaussian intensity profile at any position along the beam axis z, while the beam width and radius of curvature are continuously changing. Figure 2.1 illustrates the variation of the parameters of a focused beam along the

propagation distance z. Figure 2.2 shows an image of an experimentally generated Gaussian beam. The coloured rings in the image displayed illustrate the intensity distribution of the beam.

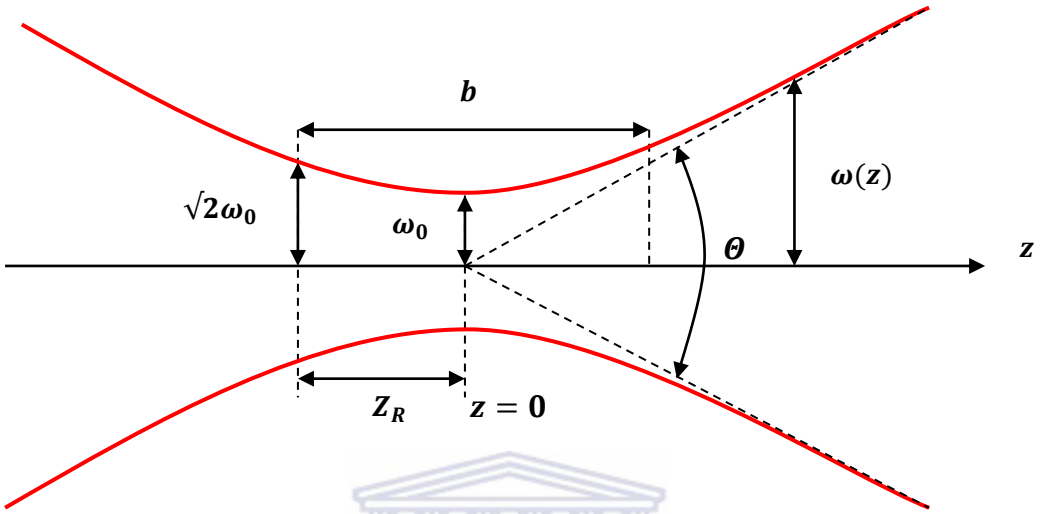

Figure 2.1: A diagram illustrating the Gaussian beam width $\omega(z)$ as a function of the axial distance z, the beam waist ω_0, the depth of focus b , Rayleigh range z_R, and the total angular spread Θ [13].

UNIVERSITY of the
WESTERN CAPE

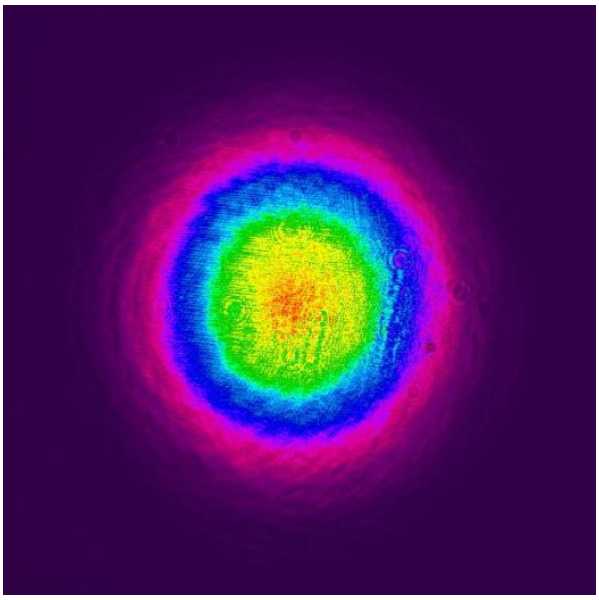

Figure 2.2: Image of an experimentally generated Gaussian beams.

The complex electric field amplitude of a Gaussian beam is given by [14]

$$U(r,z) = U_0 \frac{\omega_0}{\omega(z)} \exp\left[-\left(\frac{r}{\omega(z)}\right)^2\right] \exp\left(-i\left[kz - \arctan\frac{z}{z_R} + \frac{kr^2}{2R(z)}\right]\right), \quad (2.1)$$

where $U_0 = A_1/iz_R$ is the peak amplitude, r is the radial coordinate, $\omega(z)$ is the beam width, ω_0 is the beam waist, $k = 2\pi/\lambda$ is the wavenumber, z_R is the Rayleigh range, and $R(z)$ is the radius of curvature of the wavefront [13]. The functions $\omega(z)$, $R(z)$, and $\phi(z)$ deserve special attention and are described in the following sub-sections.

The intensity of the Gaussian beam in Fig. 2.3 is then given by the square of the complex electric field amplitude function as,

$$I(r,z) = |U(r,z)|^2 = I_0 \exp\left[-2\left(\frac{r}{\omega(z)}\right)^2\right]. \quad (2.2)$$

Here I_0 is the maximum intensity of the beam and it is defined as follows

$$I_0 = \frac{2P_0}{\pi\omega^2(z)}, \quad (2.3)$$

where P_0 is the total optical power of the laser.

UNIVERSITY of the
WESTERN CAPE

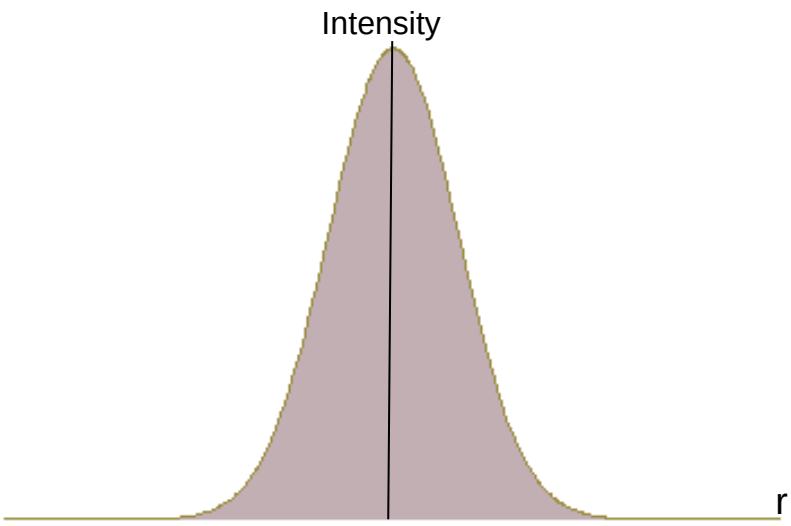

Figure 2.3: Intensity profile of a Gaussian beam.

2.2.1 Propagation Parameters

Figure 2.1 suggests that the important parameters that describe the propagation of the Gaussian beam include beam waist, beam width, Rayleigh range, depth of focus, radius of curvature and axial distance. A Gaussian beam has a transverse phase profile described by a polynomial of second order. The linear phase variation of the beam describes the tilt, while the quadratic phase variation describes either the convergence or divergence of the beam [13].

UNIVERSITY of the
WESTERN CAPE

2.2.1.1 Beam width

The beam width $\omega(z)$ is defined as the distance across the beam where the intensity decreases to $1/e^2$ or (13.5%) of the maximum I_0 value. The beam width varies as the Gaussian beam propagates along an optical axis z as [12, 13],

$$\omega(z) = \omega_0\sqrt{1 + \frac{(z-z_0)^2}{z_R^2}}, \tag{2.4}$$

where z_0 is the position of the beam waist and $z_R = \frac{\pi\omega_0^2}{\lambda}$ is the Rayleigh range. The Rayleigh range determines the length over which the beam can propagate

without diverging significantly. The beam propagates with minimal divergence when $z < z_R$. As seen in Fig. 2.1 the beam width reaches its minimum at the waist and expands thereafter.

2.2.1.2 Divergence

Laser beam divergence is defined as a measure of how fast the beam expands far from the beam waist i.e. in the far field.

In the far-field, when $z \gg z_R$, the beam width approaches the value [12, 13]

$$\omega(z) \cong \frac{\lambda z}{\pi \omega_0}. \tag{2.5}$$

When $z \gg z_R$ from Eq. 2.5, it is observed that the boundary describing the beam width asymptotically approaches a cone with an angle of,

$$\theta \cong \frac{\omega(z)}{z} = \frac{\lambda}{\pi \omega_0}. \tag{2.6}$$

UNIVERSITY of the
WESTERN CAPE

This angle is known as the divergence of a Gaussian beam and describes how the beam spreads out as it propagates. It is clearly seen that the divergence and the waist of the fundamental beam are inversely proportional. Therefore in order to obtain a well collimated beam, the fundamental beam width must be large [13].

2.2.1.3 Radius of Curvature

The electric field given in Eq. (2.1) is a complex function. The last term of the imaginary component in the exponential function has a quadratic dependence on the radial component r. The radius of curvature is defined as [12, 13]

$$R(z) = (z - z_0)\left[1 + \left(\frac{z_R}{z - z_0}\right)^2\right], \tag{2.7}$$

and it is referred to as the radius of curvature of the wavefront of a Gaussian beam.

The term with the $arctan$ function in the imaginary exponential part of Eq. (2.1) describes the Gouy phase shift, $\phi(z)$. The Gouy phase shift is important for the resonance frequencies of the optical resonators. Along the z direction, a Gaussian beam attains the Gouy phase shift, which is different from that of a plane wave with the same optical frequency, given by [12-14],

$$\phi(z) = \arctan\left(\frac{z}{z_R}\right). \tag{2.8}$$

This shift causes the distance between the wavefronts to increase slightly as compared with that defined for a plane wave of the same frequency.

UNIVERSITY of the
WESTERN CAPE

2.3 Bessel Beams

Research has shown the existence of beams that do not experience diffractive spreading [9, 10] and these beams are referred to as 'non-diffracting' beams. All diffractive occurrences can be described by the Helmholtz equation:

$$[\nabla^2 + k^2]\Phi(r, k) = 0. \tag{2.9}$$

Durnin in 1987 discovered Bessel beams as exact solutions to the free-space Helmholtz's wave equation, described by Bessel functions which are not subject to transverse spreading [9-10]. In particular, these solutions describe well-defined beams with narrow central beam waist, which do not display diffractive spreading for over long propagation distances [9, 12].

Bessel beams are formed as a result of the interference of plane waves propagating along a conical surface. A region of self-interference develops in which a Bessel pattern forms due to cylindrical symmetry [7]. An ideal Bessel beam contains an infinite number of rings over an infinite area and thus carries infinite energy which therefore cannot be generated experimentally [15-18]. However it is possible to generate finite size approximations to Bessel beams [18-21] which can propagate over extended distances in a diffraction free manner.

These finite Bessel beams are known as quasi-Bessel beams and they are characterized by a transverse electric field component [17]

$$E(r,\varphi,z) = A_0 J_l(k_r r)\mathrm{e}^{i(k_z z + l\varphi)}, \tag{2.10}$$

where J_l is the lth order Bessel function, z is the coordinate in the propagation direction, r and φ are the transverse and polar coordinates, k_z and k_r are the longitudinal and transverse wave numbers respectively [9, 17].

UNIVERSITY of the
WESTERN CAPE

The zero-order $(|l| = 0)$ Bessel beam has a bright central core surrounded by concentric rings while higher-order $(|l| > 1)$ Bessel beams have a dark central core due to a phase singularity arising from the azimuthal phase term $\exp(il\varphi)$ [15]. Bessel beams of different orders are shown in Fig. 2.4 ranging from zero order to the third order.

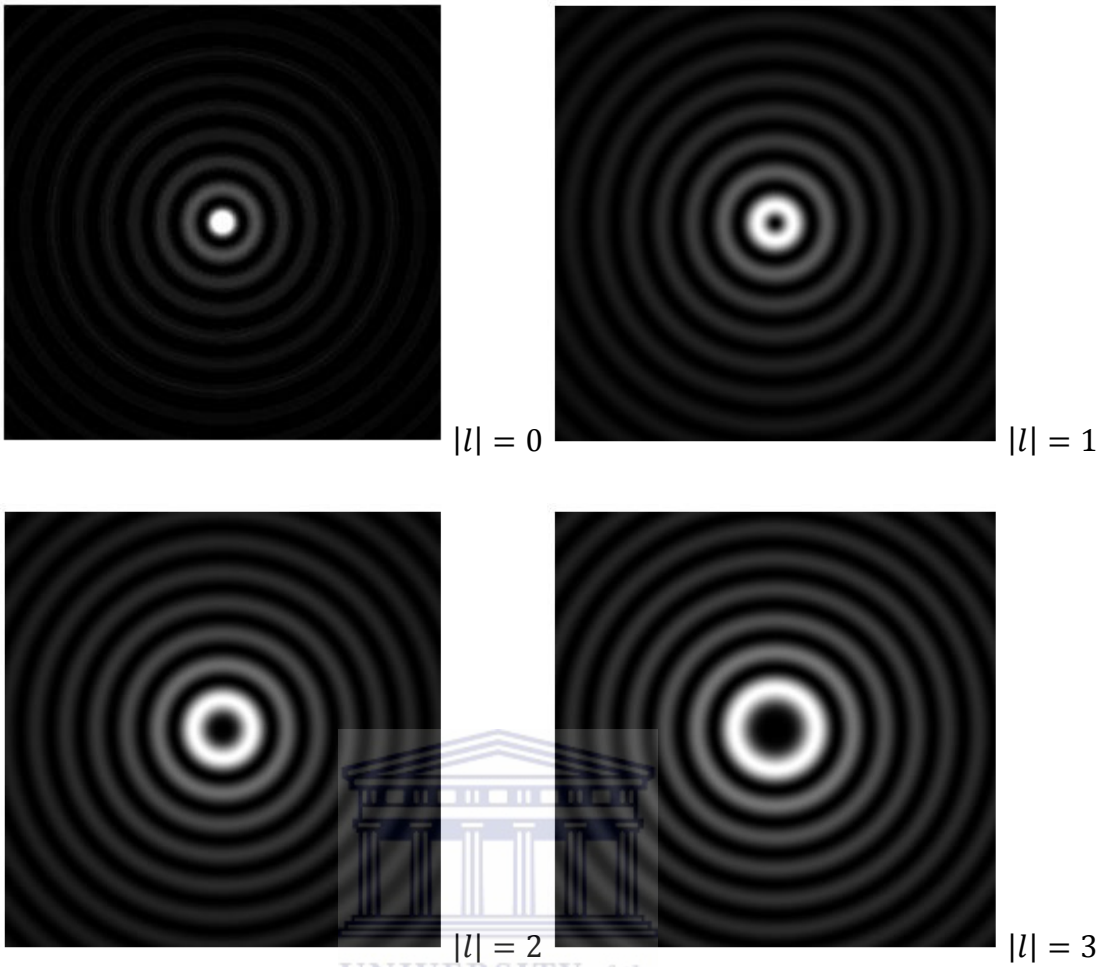

UNIVERSITY of the
WESTERN CAPE

Figure 2.4: Theoretical generated intensity profiles of a zero-order $(|l| = 0)$ and higher order $(|l| > 1)$ Bessel beams.

In the far field of the Bessel beam, the separation between the wave-vectors increases while the beam intensity in the central axis decreases and it eventually becomes null. This then corresponds to an annular beam [7]. The intensity profile of an annular ring and the annular ring are shown in Fig. 2.5.

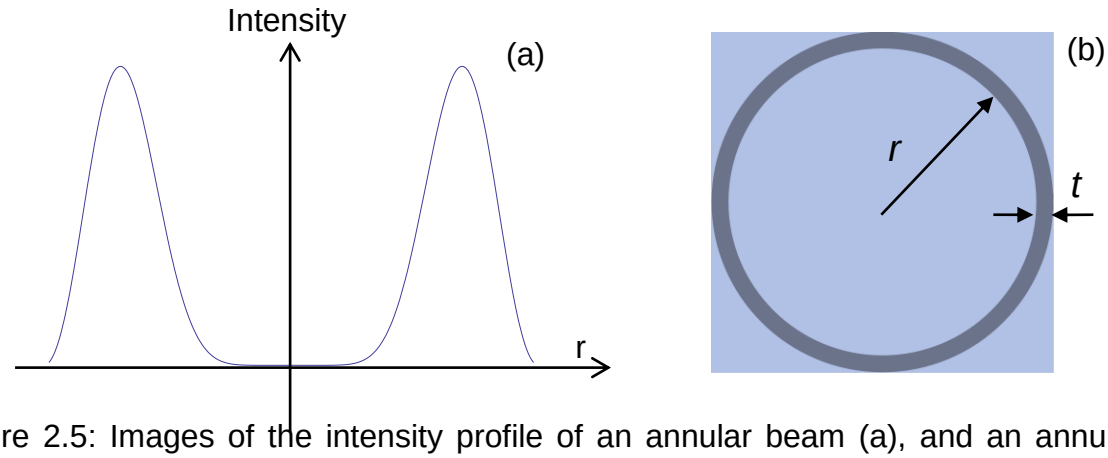

Figure 2.5: Images of the intensity profile of an annular beam (a), and an annular ring (b), with radius *r* and thickness *t*.

One of the optical properties of a Bessel beam is its ability to reconstruct after encountering an obstruction on its central core [18], this property is commonly known as self-healing. The self-healing concept is understood by taking into account that Bessel beams are constructed as a superposition of plane waves propagating on a cone. If an object is placed in the centre of the beam, the waves that create the beam are able to move past the obstruction resulting in a shadow being cast into the beam [15, 18]. The light waves that form the beam move along the outer sides of the cone and are thus not affected by what happens in the centre of the propagation region [20-22].

This unique property can help to mitigate effects of debris and other products associated with laser processing that can partially block incident beams. Durnin et.al [9] showed that Bessel beams exhibit a greater depth of field than that of Gaussian beams and their Rayleigh range is longer than that of Gaussian beams. A major disadvantage to having an extended depth of field is that the optical energy is distributed among the rings leading to loss in power and contrast.

2.3.1 Generation of Bessel Beams using axicons

There are two well established methods for Bessel beam formation, one makes use of the annular slit [9] and the other makes use of the axicon [23]. Others include aperture based methods, a spatial light modulator (SLM) [7], a tuneable acoustic gradient (TAG) lens, and optical fibres [7]. A Bessel beam can be visualised as a superposition of plane waves whose vectors lie on a cone, which translate into a ring in the *k*-space, i.e. the Fourier transform of a ring results in a Bessel beam and vice versa.

Durnin et al. [9] were the first to produce Bessel beams experimentally. They placed an annular slit at the back focal plane of a focusing lens, and illuminated the slit with a plane wave. This method proved to be inefficient since most of the incident radiation was blocked by the aperture. This loss of energy is unsuitable for material processing applications since high intensities are required [9-10].

UNIVERSITY of the
WESTERN CAPE

Generating Bessel beams with the use of axicons is considered as the most common, cost-effective and convenient method as it offers the prospect of high conversion efficiencies [2, 24]. However, the alignment between the incident laser beam and the axicon is a critical issue because it can result in non-uniformities in case of misalignment [10].

An axicon, (commonly referred to as a rotationally symmetric prism or conical lens) is a specialized type of lens which features one conical surface and one plano surface. It can be used to image a point source into a line along the optic axis or to transform a laser beam into a ring [23]. When transforming a collimated beam into a ring the plano side faces the collimated source. Figure 2.6 shows a typical image of an axicon, most of these are made from high-quality fused silica using computer numerical controlled (CNC) grinding and polishing machines. The fused silica provides a high-quality surface which then makes them ideally suited for high-power laser applications. They are most commonly manufactured with base angles γ, which range from 0.5° to 20° [25]. The axicons have an anti-reflection coating which reduces surface reflections from the lens to maximise transmission [2].

Figure 2.6: An image of an axicon with a plano surface on one side and a conical surface on the other [25].

Figure 2.7 illustrates how a Bessel beam is created by illuminating the axicon with a Gaussian beam. The opening angle of the cone, θ, on which the wave vectors of the Bessel beam propagate is given by,

$$\theta = (n - 1)\gamma, \tag{2.11}$$

where n is the refractive index of the axicon and γ is the base angle of the axicon. A Gaussian beam passes through an axicon to form a Bessel beam which at the far field becomes an annular ring as shown in Fig. 2.7.

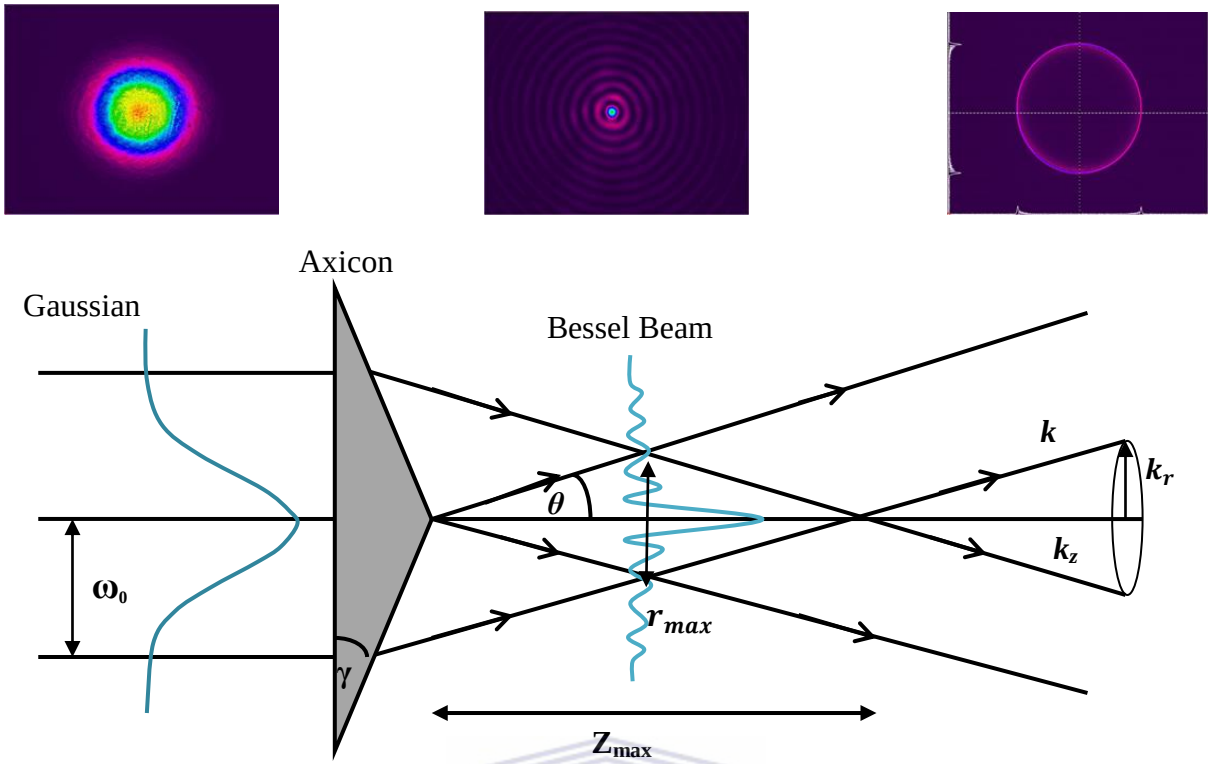

Figure 2.7: A diagram illustrating the finite propagation distance of a Bessel beam generated by illuminating a Gaussian beam onto an axicon with an opening angle θ [15].

UNIVERSITY of the
WESTERN CAPE

When illuminated by a Gaussian beam, axicons generate Bessel beams with a long depth of field and a sharp central spot, this intense central spot is surrounded by concentric rings of much lower intensity. A Bessel beam is thus produced through the interference of all parts of the incident beam that have been refracted at the same opening angle θ by the axicon [26-31].

The intensity distribution of a collimated Gaussian beam passing through an axicon can be calculated with the Fresnel-Kirchhoff integral and it is given by the relation [7, 9]

$$I(r,z) = 2\pi k(\tan^2\gamma)(n-1)^2 z I_0 \mathrm{e}^{2\left(\frac{(n-1)z\tan\gamma}{\omega_0}\right)^2} \times J_0^2(k(n-1)r\tan\gamma), \quad (2.12)$$

where r and z are the radial and longitudinal coordinates respectively, I_0 is the incident on-axis intensity, ω_0 is the incident beam waist, k is the wavenumber, n is the refractive index of the axicon and γ is the base angle of the axicon.

The area marked z_{max} in Fig. 2.7 is the diffraction-free beam formation zone where the main lobe of the beam retains a small diameter. z_{max} is the finite propagation distance of a Bessel beam, this finite propagation distance is approximated for small angles by the ratio of the beam waist ω_0 and the opening angle θ [1, 22]. z_{max} is given by

$$z_{max} = \frac{k}{k_r}\omega_0 \approx \frac{\omega_0}{\theta}. \tag{2.13}$$

Within this finite propagation distance, the properties of an ideal Bessel beam hold true for the experimentally obtained Bessel beam. Using geometric optics, further information about the beam can be revealed. Fig 2.8 illustrates how and where the maximum width of the Bessel beam is obtained. The maximum width, r_{max}, is found at $z_{max}/2$:

$$r_{max} = z_{max}\tan\theta. \tag{2.14}$$

UNIVERSITY of the
WESTERN CAPE

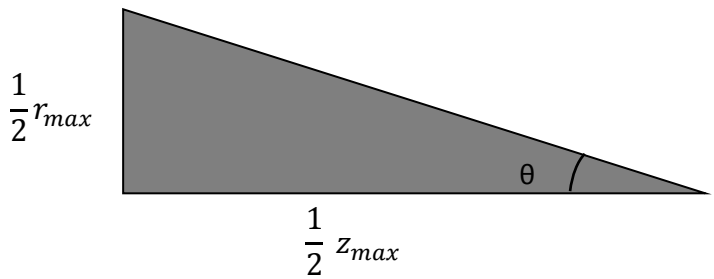

Figure 2.8: A diagram that illustrates the relationship between r_{max} and z_{max}

The number of rings is dependent on the incident Gaussian beam waist and the base angle of the axicon. The total number of rings is found at r_{max} and the expression used to calculate the number of rings in a Bessel beam is given by [15]

$$N = \frac{r_{max}}{2}\frac{1}{\delta}, \tag{2.15}$$

where δ is the spacing between the rings and it is given as $\delta = \frac{\pi}{k_r}$.

The central spot for a zero order Bessel beam has the highest intensity and it is thus brighter. The base angle γ of an axicon determines the waist and the extent of the central spot of the Bessel beam [1]. A smaller cone angle corresponds to a wider central spot and a longer "diffraction-less" propagation zone. Equation (2.12) together with the properties of the zero order of a Bessel function can be used to determine the size of the central core spot given by [17]

$$r_0 = \frac{2.405}{k_r}. \tag{2.16}$$

Axicons can be used to also generate annular beams. This can be done in two ways, firstly the plane of reference is viewed at a distance far enough from the axicon so as to encounter the far-field profile of the axicon which corresponds to an annulus. The second method would require the combination of an axicon with another focussing element, (i.e. lens, axicon or microscopic objective) to create an annulus at the focal plane of the system. The outer diameter of the annulus generated using an axicon and a lens is determined from the Fresnel theory. From Fresnel theory the field at a distance *f* away is given by

$$U_1(\rho) = \frac{k}{f}\exp\left[i\left(kf - \frac{\pi}{2} + \frac{k\rho^2}{2f}\right)\right]\int_0^\infty U_0(r)J_0\left(\frac{k_r\rho}{f}\right)rdr, \tag{2.17}$$

where ρ is the radius of the ring.

In this case the initial field is a Bessel field, thus

$$U_0(r) = J_0(\gamma r). \tag{2.18}$$

So Eq. (2.17) can be written as

$$U_1(\rho) \propto \frac{k}{f}\int_0^\infty rJ_0(\gamma r)J_0\left(\frac{k_r\rho}{f}\right)dr. \tag{2.19}$$

It is known from the orthogonality of Bessel functions that

$$\int_0^\infty xJ_0(ux)J_0(vx)dx = \frac{1}{u}\delta(u-v), \tag{2.20}$$

thus Eq. (2.19) becomes

$$U_1(\rho) \propto \frac{k}{f} \times \frac{1}{\gamma}\delta\left[\gamma - \frac{k\rho}{f}\right]. \tag{2.21}$$

The intensity of the field is then given by

$$I_1 = |U_1|^2 = \frac{k^2}{f^2\gamma^2}\delta\left[\gamma - \frac{k\rho}{f}\right], \tag{2.22}$$

$$\delta\left[\gamma - \frac{k\rho}{f}\right] \neq 0 \text{ only when } \rho = \frac{\gamma f}{k}, \tag{2.23}$$

So the radius of the ring is:

$$\rho_{ring} = \frac{\gamma f}{k}. \tag{2.24}$$

UNIVERSITY of the
WESTERN CAPE

The diameter of the ring depends on the focal length of the lens, the index of refraction n, and the opening angle of the cone θ. A physical illustration on the measurement of the diameter of the ring is illustrated in Fig. 2.9. It is observed that the thickness of the ring t remains constant throughout the propagation, and it is equivalent to the radius of the initial beam or one half of the beam's diameter, $t = \omega_0$. From Fig. 2.9, Eq. (2.24) can be written as $d_r = 2L\tan\theta$, where L is the distance between the tip of the axicon and the image plane, d_r is the ring diameter. By increasing the length from the axicon output to the imaging plane, the diameter of the ring increases, while t remains the same.

However for image capturing processes, a lens is introduced and placed in the propagation zone. This is done in order to bring the far field closer for analysis using a camera. The camera is used as the imaging plane and L becomes the focal length of the lens used. This will be further discussed in subsection 2.4.3.

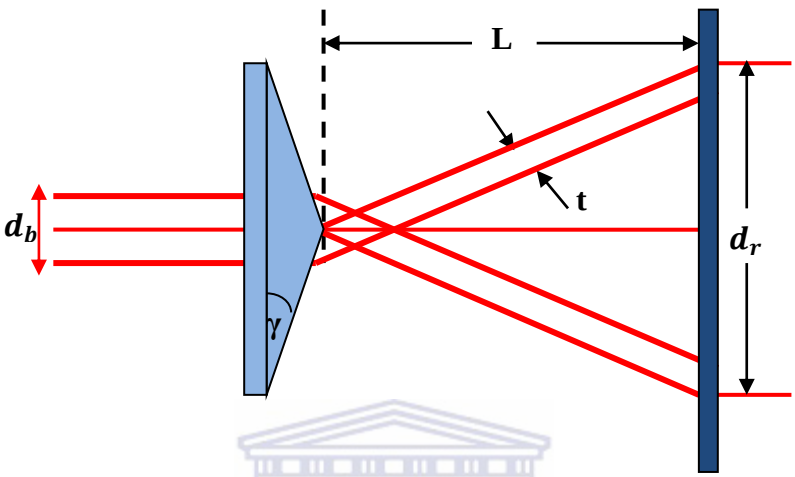

Figure 2.9: A diagram illustrating the formation of an annular beam with diameter d_r, ring thickness t, and a length L away from the tip of the axicon.

UNIVERSITY of the
WESTERN CAPE

2.4. Experimental procedure for generation and characterisation of Bessel and annular beams

Experiments were conducted to measure the properties that defines Bessel beams viz. z_{max}, r_0, and ρ_{ring}. Various optical instruments were used and they are described in the subsections below. Experimental setups include that for generating first order Bessel beams and their annular beams.

2.4.1 Experimental setup using an axicon

Zero order Bessel beams were generated by illuminating an axicon ($\gamma = 5°$, and $n = 1.5$) with a Gaussian beam emitted from a cw fiber laser (IPG Photonics YL Series), operated at a central wavelength of $\lambda = 1064$ nm and output power of

50 W. The laser emits a collimated Gaussian beam with width $\omega(z) = 1.67 \pm 0.01$ mm. Figure 2.10 shows a schematic diagram of the experimental setup and optical elements used to generate zero-order Bessel beams.

A CCD camera (model Ophir-Spiricon USB 2.0) together with the BeamGage beam analyser software was used to view the beam and measure its properties. Mirrors are used to guide the laser beam in its optical path, and Neutral density (ND) filters are used to attenuate the intensity of the beam in order to avoid saturation on the camera. The beam appears small in size on the camera, thus a magnification system is required for beam measurements. The magnification system is discussed in section 2.4.2.

UNIVERSITY of the
WESTERN CAPE

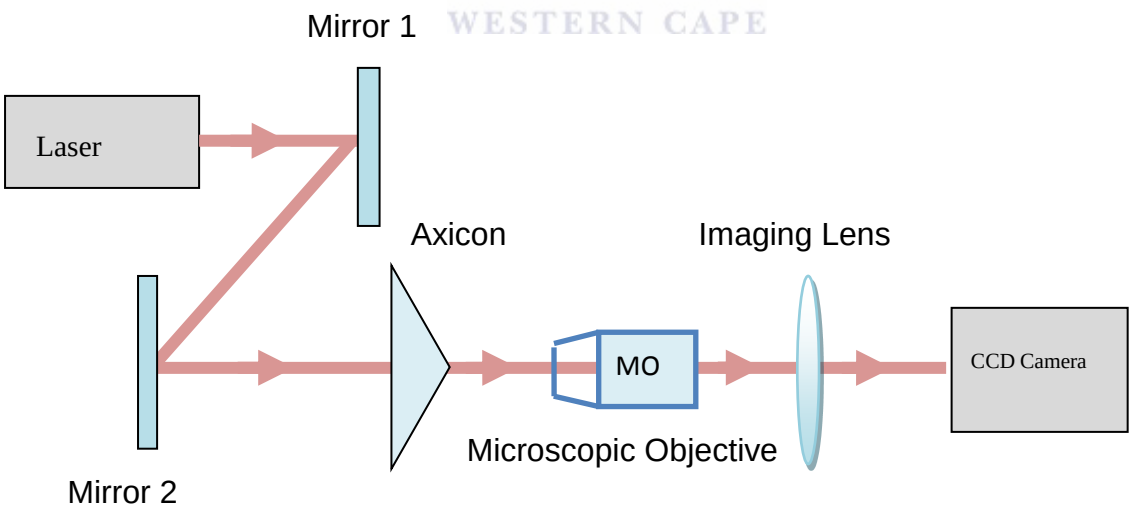

Figure 2.10: Experimental setup for generating zero order Bessel beams using an axicon.

2.4.2 Magnification system

A 10X microscopic objective (MO) was used to magnify the Bessel beam onto the camera. The 10X MO has a working distance (WD) of 10.5 mm and a focal distance (FD) of 18 mm. Figure 2.11 illustrates the magnification system used to view and analyse the beam properties. The system in Fig 2.11 has a magnification M of 11X, this was obtained by dividing the focal length of the lens by the focal distance of the MO. The MO, lens and the camera were mounted on a rail, with the camera placed at the focal distance of the lens. The distance between the MO and the lens is referred to as the infinity space hence its distance can be varied, in this system it was measured to be 135 mm [32]. The front side of the MO is placed 10.5 mm (working distance) from the plane of reference, this means that if one has to view the beam at half z_{max}, the front part of the MO will be placed at distance $\frac{1}{2}z_{max}$+WD.

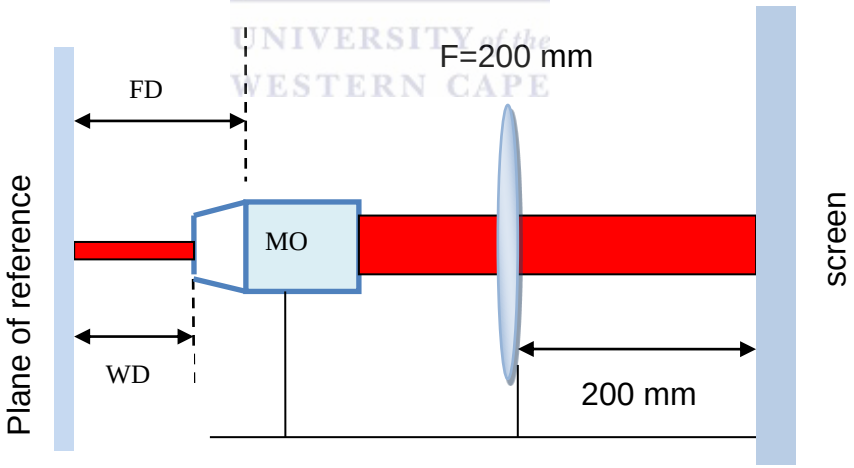

Figure 2.11: A diagram that illustrates the imaging and magnification system using a microscopic objective and a lens.

2.4.3 Experimental setup for generating an annular beam.

Figure 2.11 is a schematic diagram of the experimental setup used to generate an annular ring. As mentioned above, the Fourier transform of a Bessel beam is an annular ring, a lens ($f = 60$ mm) was used to Fourier transform the Bessel beam. The plane of reference being imaged by the lens is at half z_{max}, thus the lens was placed at its focal distance (60 mm) plus the half z_{max} (18.34 mm), distance away from the tip of the axicon. A microscopic objective can be used to demagnify the annular beam if it is too large to fit on the CCD camera screen. The MO is placed in front of the lens in a back to front direction.

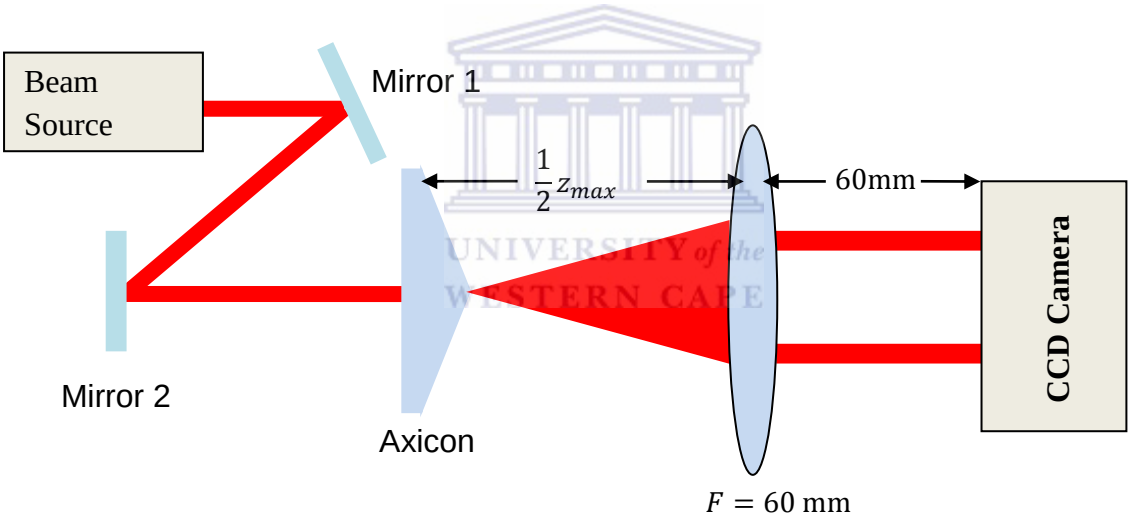

Figure 2.12: A diagram illustrating the experimental setup for generating an annular ring. The camera is placed at the focal distance of the lens. The lens is place at r_{max} of the Bessel beam.

2.5 Results and discussion

Zero-order Bessel beams were generated using the experimental setup in Fig. 2.10. A zero order Bessel beam has a central bright spot surrounded by concentric rings with equal spacing between the rings. The central spot has the highest peak intensity, however the intensity drops as one moves away from the central spot. The x and y intensity profile can be seen in Fig. 2.13 (a).

From Fig. 2.7, the Bessel beam formation is observed from the tip of the axicon, while experimentally the formation zone is observed a few millimetres away from the tip. The offset distance measured was approximately 6 mm away from the tip of the axicon. As seen in Fig. 2.14 (a)-(p) the first outer ring is visible at about 7 mm away from the tip of the axicon. The number of rings increases along the propagation distance and reaches its maximum at half z_{max} and the total number of rings can be calculated using Eq. 2.15.

UNIVERSITY of the
WESTERN CAPE

The Bessel beam is profiled in a diamond shape (see Fig. 2.7), with the intensity increasing from the beginning until it reaches its maximum at half the propagation distance. The intensity decreases in the second half of the propagation distance. Ideally one would expect to see the number of rings reducing along the second half of the propagation distance; however this is not the case. Instead the rings fade away from the inside and as one moves toward the end of the propagation zone, only the very most outer rings are visible (see figure 2.15).

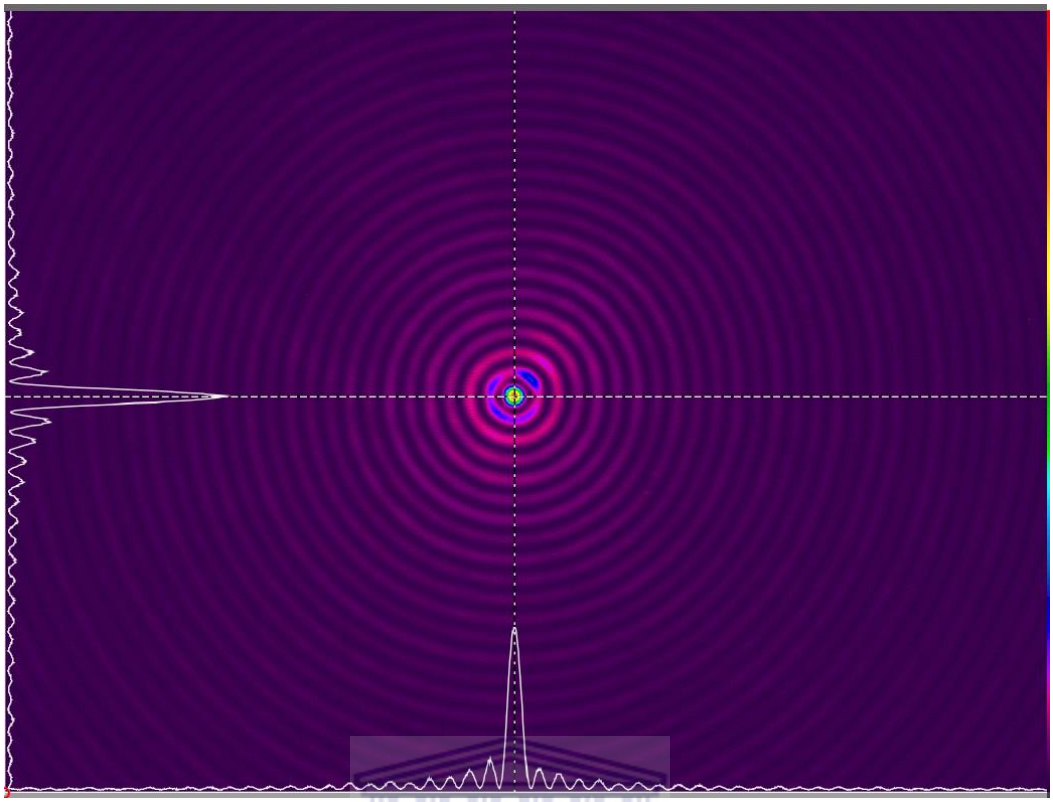

(a)

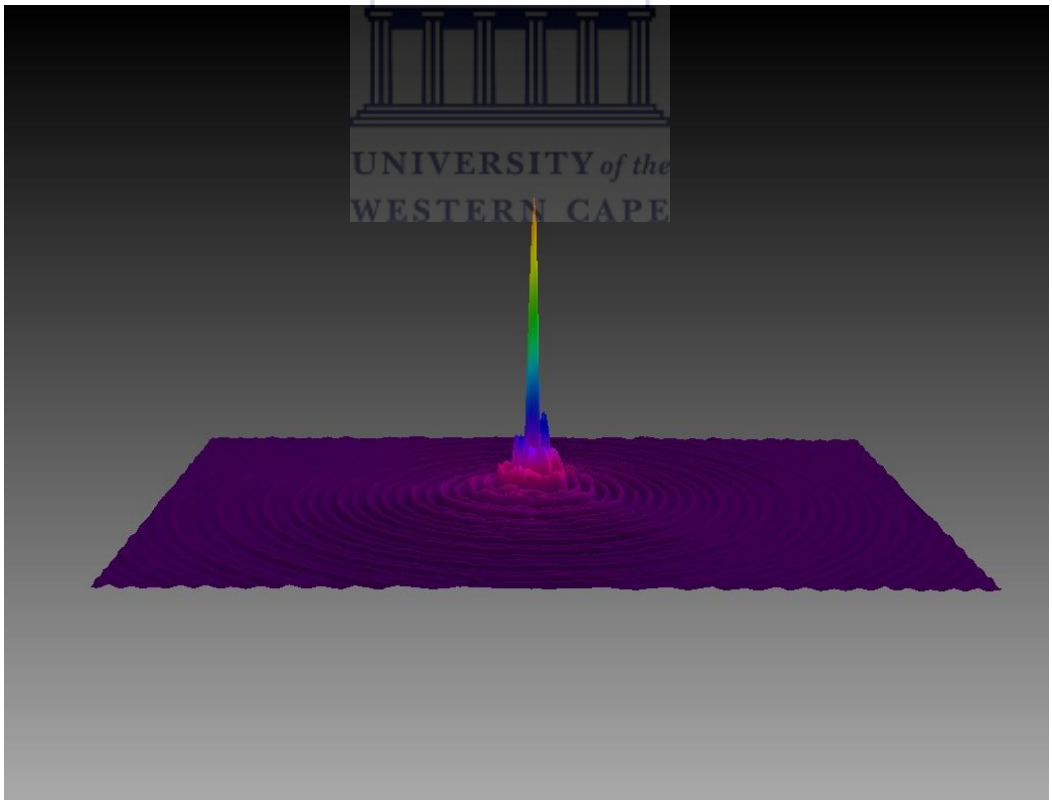

(b)

Figure 2.13: A zero-order experimentally generated Bessel beam, (a) 2D image profile and (b) 3D image profile.

UNIVERSITY of the
WESTERN CAPE

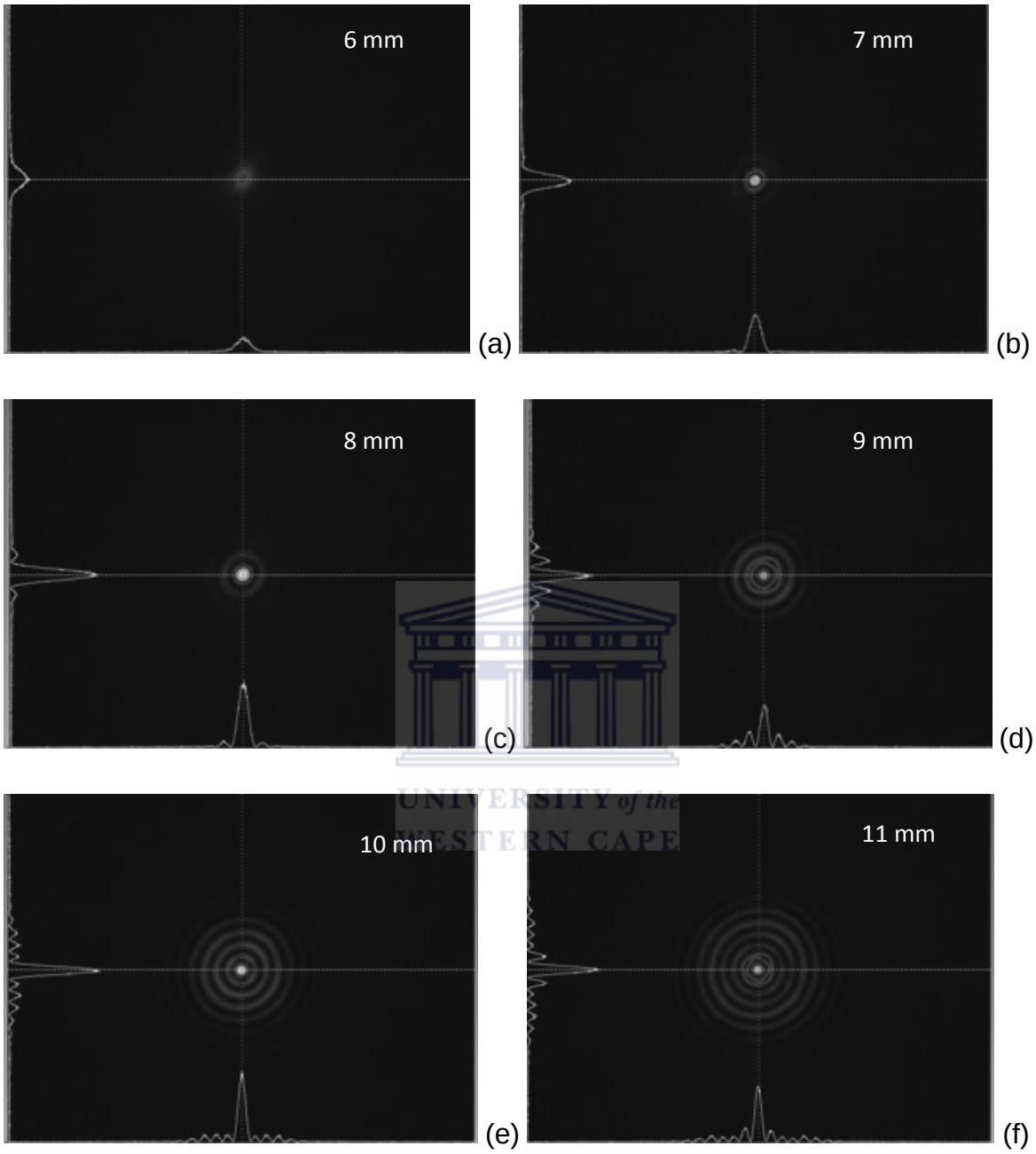

UNIVERSITY of the
WESTERN CAPE

Figure 2.14 (i): A series of experimental results, displaying images of Bessel beams along the propagation distance created using an axicon with opening angle $\gamma = 5^{\circ}$ and a Gaussian beam with beam width $\omega(z) = 1.67$ mm. Imaged at distances 6 mm to 11 mm away from the tip of the axicon.

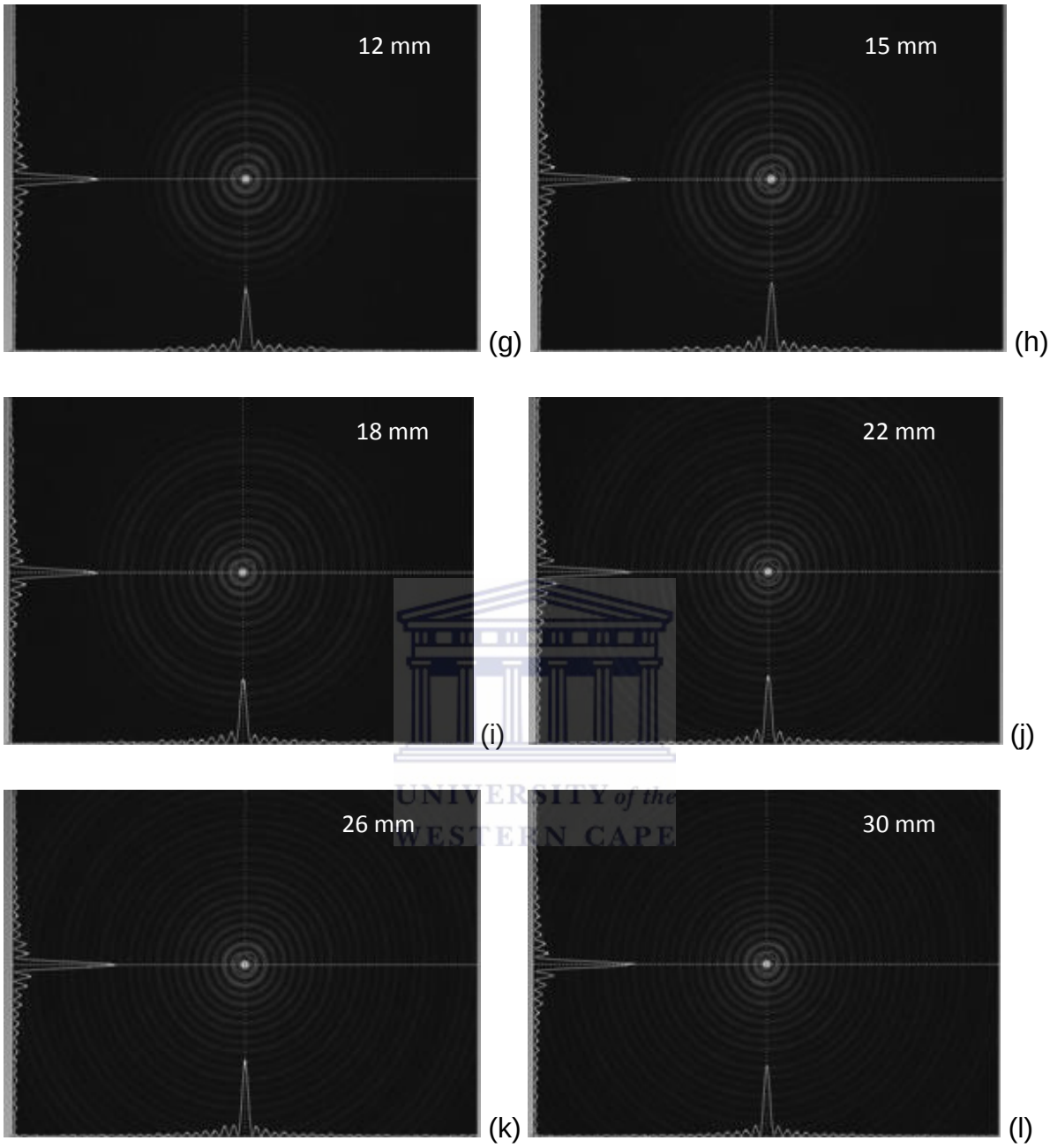

Figure 2.14 (ii): A series of experimental results, displaying images of Bessel beams along the propagation distance created using an axicon with opening angle $\gamma = 5^{\circ}$ and a Gaussian beam with beam width $\omega(z) = 1.67$ mm. Imaged at distances 12 mm to 30 mm away from the tip of the axicon.

UNIVERSITY of the
WESTERN CAPE

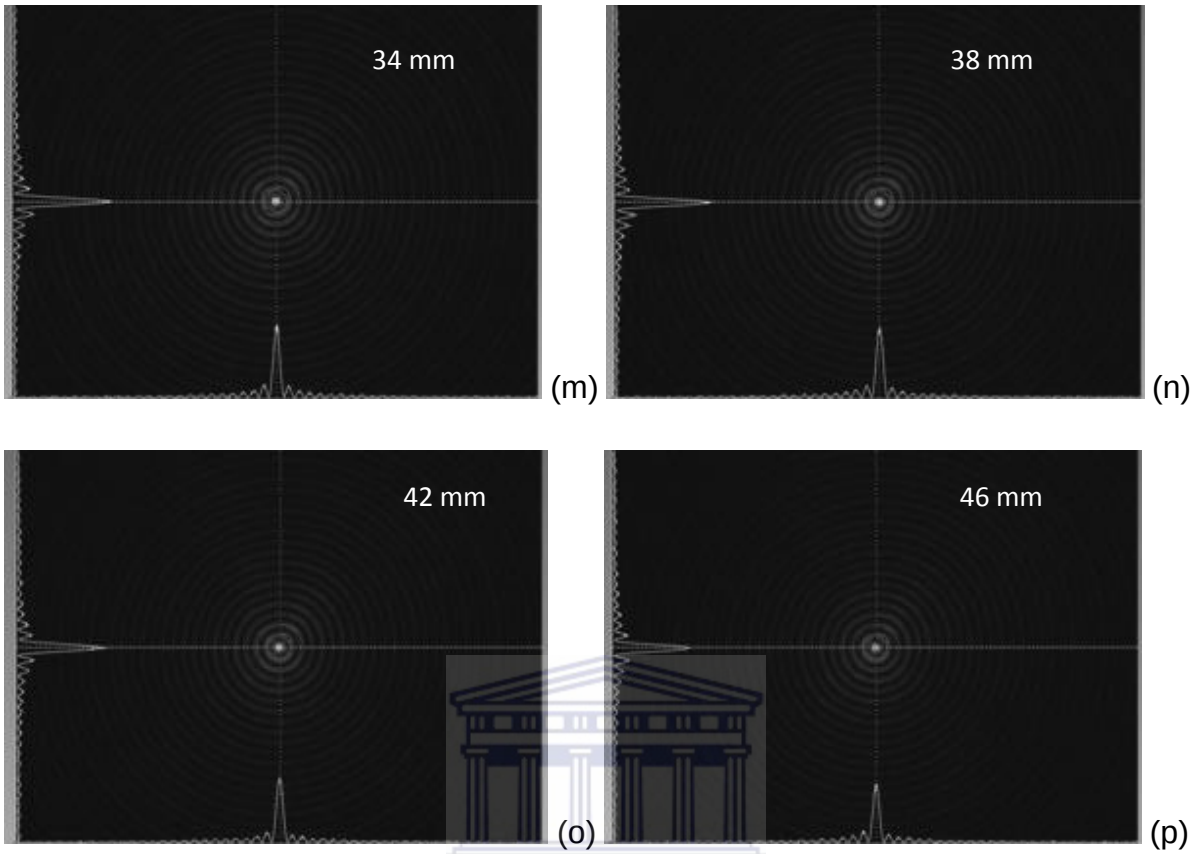

Figure 2.14 (iii): A series of experimental results, displaying images of Bessel beams along the propagation distance created using an axicon with opening angle $\gamma = 5^{\circ}$ and a Gaussian beam with beam width $\omega(z) = 1.67$ mm. Imaged at distances 34 mm to 46 mm away from the tip of the axicon.

UNIVERSITY of the
WESTERN CAPE

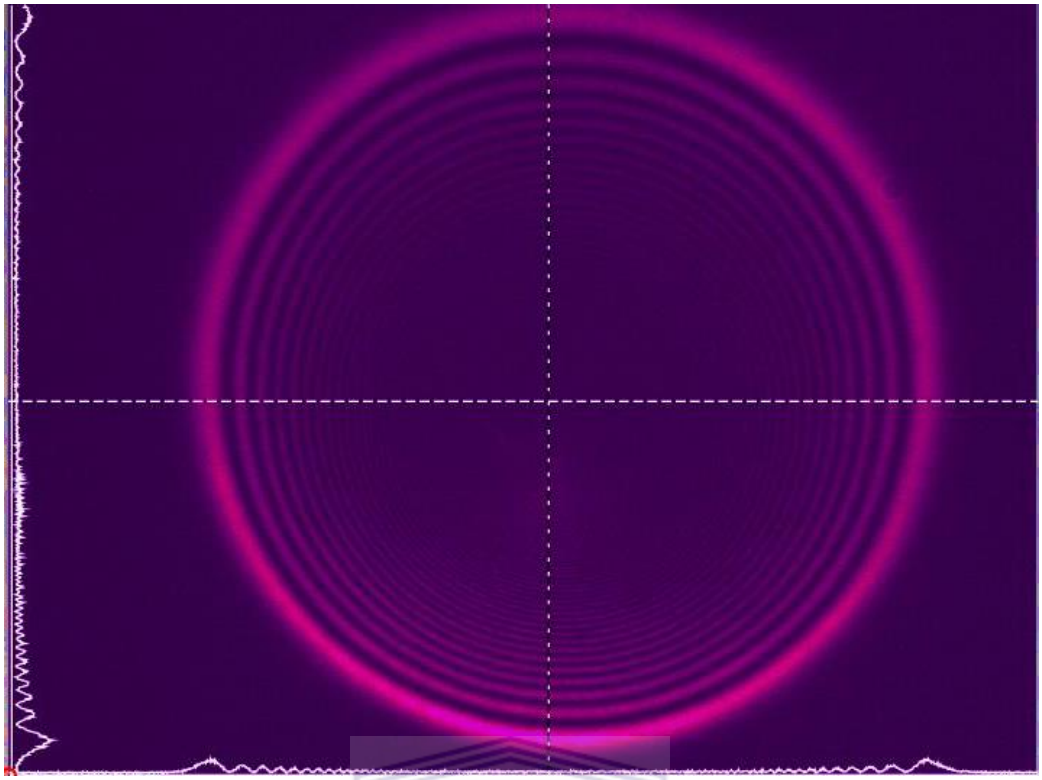

Figure 2.15: An image of a Bessel beam imaged after half z_{max} region with the rings fading from inside out.

UNIVERSITY of the
WESTERN CAPE

As stated in the above sections the Fourier transform of a Bessel beam is an annular beam. Experimentally an annular beam can be seen at the far field of the Bessel beam generation setup; however for imaging purpose the setup in Fig. 2.12 was used. The diameter of the annular ring is dependent on the focal length of the imaging lens used. An annular beam generated from the setup in Fig. 2.12 is shown in Fig. 2.16.

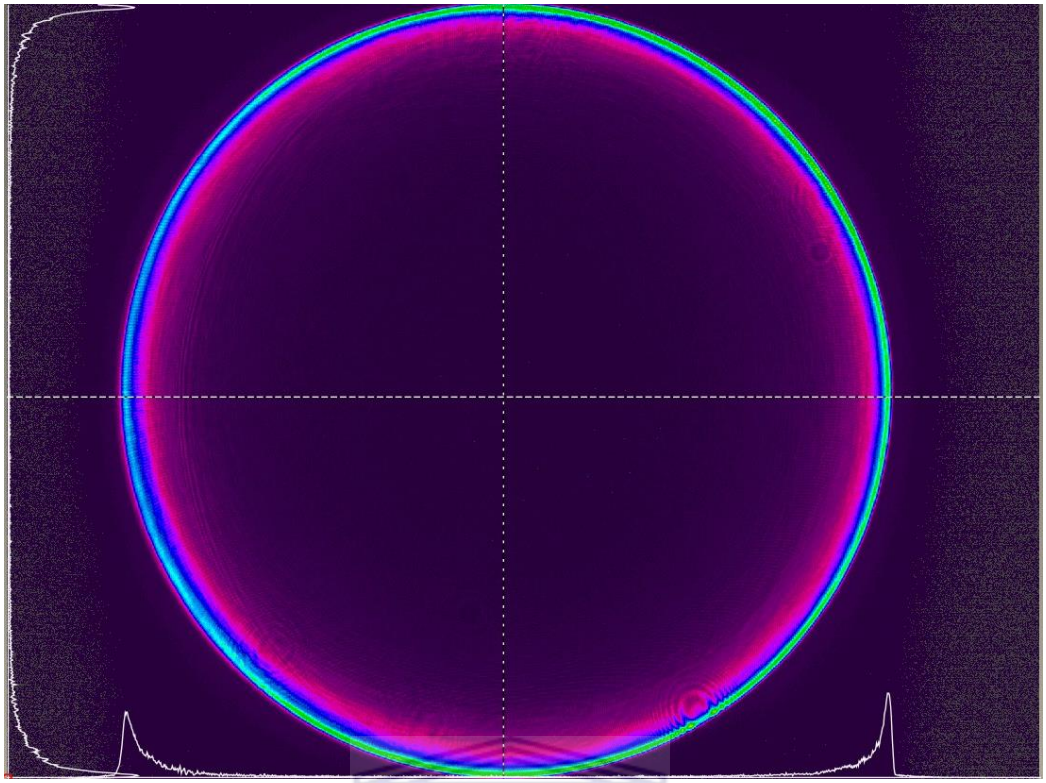

Figure 2.16: An image of an annular ring obtained from the far field of a Bessel beam.

UNIVERSITY of the
WESTERN CAPE

The Bessel beam parameters of interest that were measured include the central spot radius r_0, the propagation distance z_{max}, and the diameter of the ring. The opening angle of the cone was calculated using Eq. 2.11 to be 4.54×10^{-2} rads. This angle is linearly dependent on the base angle of the axicon, γ. The central spot radius r_0, was calculated using Eq. 2.16 to be 9.28 µm which corresponded to the measured value of $r_0 = 8.3$ µm ± 0.3 µm. The average diameter of the central spot was measured to be 16.6 µm ± 0.3 µm.

As mentioned above one of the properties of a Bessel beam is its ability to retain the same spot size over a larger focal range, this was confirmed by measuring the central spot diameter along the propagation distance. As seen in Fig. 2.17 the diameter retains almost the same size in the covered region. The difference in the central spot size along the propagation distance can be caused by the measuring system used; however the difference is accounted for with a standard deviation value of 0.3 µm. The size of the central spot is dependent on the opening angle of

the cone θ. When θ is small, the central spot size is large, this will be shown later in chapters to follow when a different axicon with a smaller γ is used to generate Bessel beams.

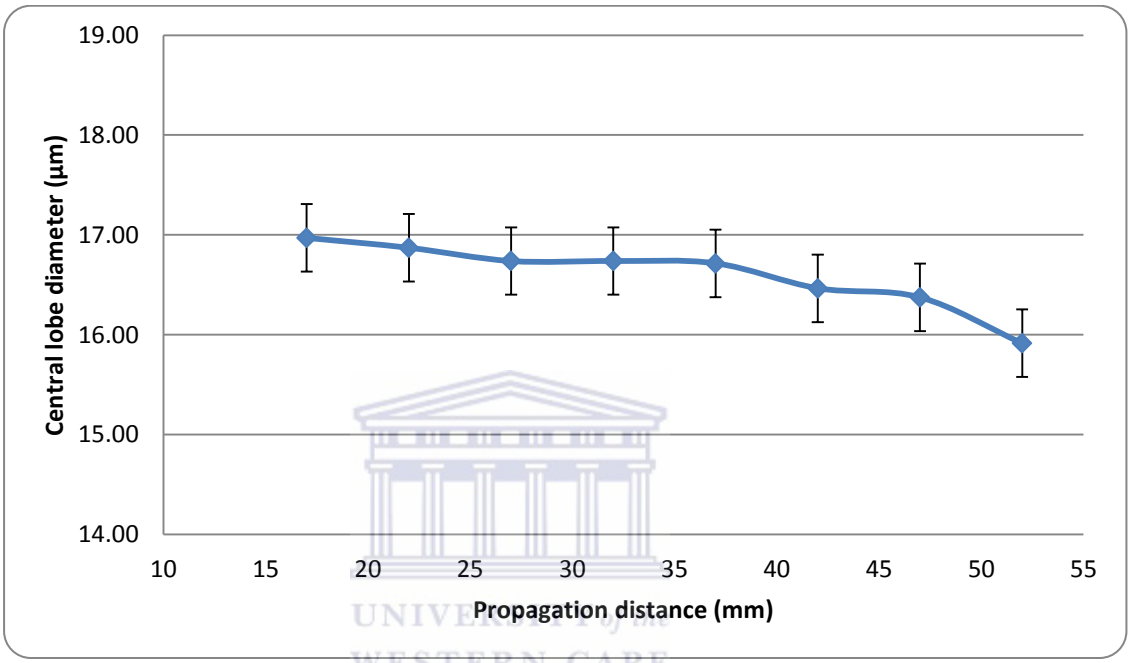

Figure 2.17: A graph illustrating the change in size of the central spot radius along the propagation distance.

The diffraction-free beam propagation zone z_{max}, is calculated from Eq. 2.13. It was a challenge to measure the full length of the propagation distance using the beam profiler mainly because of two reasons. Firstly the beam size increased and could not fit in the camera. Secondly the beam rings do not decrease in the second half of the Bessel beam region as they had increased in the first half, instead the rings fade away from the inside and the central spot's intensity decreases until it becomes null and an annular ring is visible.

To verify and compare the theoretical and experimental results, the propagation distance was measured at half its length. The calculated value $z_{max} = 36.68$ mm was then divided by half to get $\frac{1}{2}z_{max} = 18.34$ mm which corresponded closely to the measured value of $\frac{1}{2}z_{max} = 20.0$ mm ± 0.5 mm. An inverse relationship exist between z_{max} and θ. The thickness t of the annular ring is equivalent to the initial Gaussian beam radius as illustrated in Fig. 2.9. The diameter of the ring was measured to be 6.1 mm ± 0.5 mm which is close corresponds to the calculated value 5.24 mm.

The same experiments were run using a different laser with a similar setup to the one above. A Ti:Sapphire amplifier femtosecond laser (Clark-MXR CPA series) operated at a centre wavelength of $\lambda = 775$ nm, pulse duration of $\tau = 150$ fs (FWHM), average power of 1.1 W, and pulse repetition rate of 1 kHz was used to generate Bessel beams. The beam width for this laser was measured to be $\omega_0 \approx 2.55$ mm. The radius r_0 and $\frac{1}{2}z_{max}$ were calculated and measured. Figure 2.18 (a) is the initial beam profile that was illuminated onto the axicon and Fig. 2.18 (b) is the resulting Bessel beam.

UNIVERSITY of the
WESTERN CAPE

The femtosecond laser used has a poor Gaussian beam profile, although it has a beam quality of $\mathrm{M}^2 = 1.4$. The beam emitted displays more of an elliptical shape than an expected circular shape. The instability of the amplifier system causes the beam profile to be unstable losing its initial shape during the use of the laser. The elliptic shape of the initial beam has an impact on the Bessel beam, causing the intensity in the first surrounding ring to not be uniformly distributed.

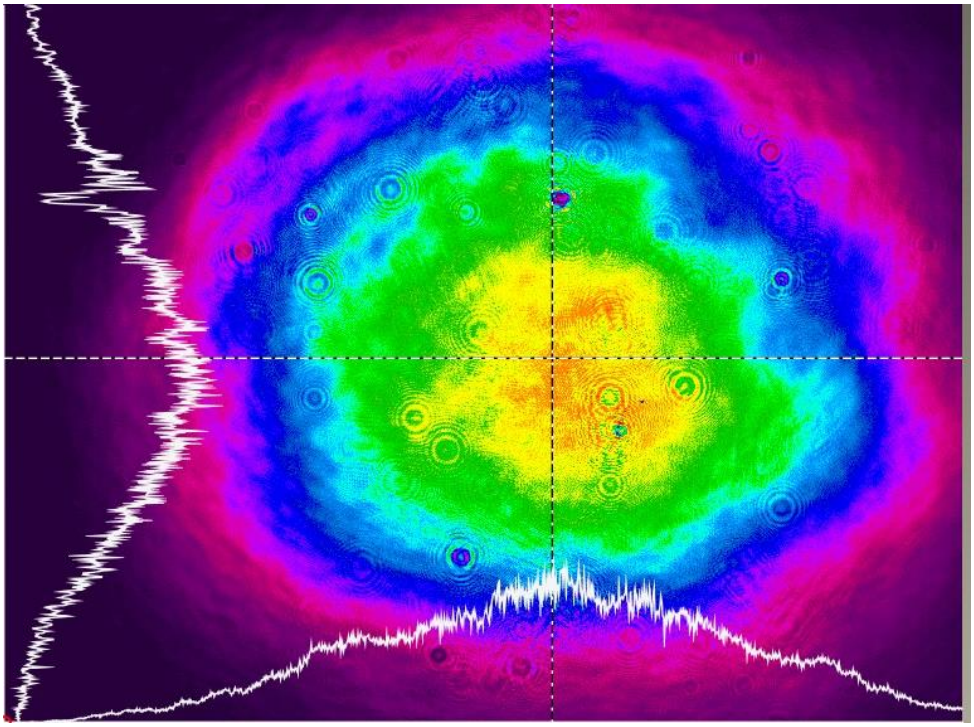

(a)

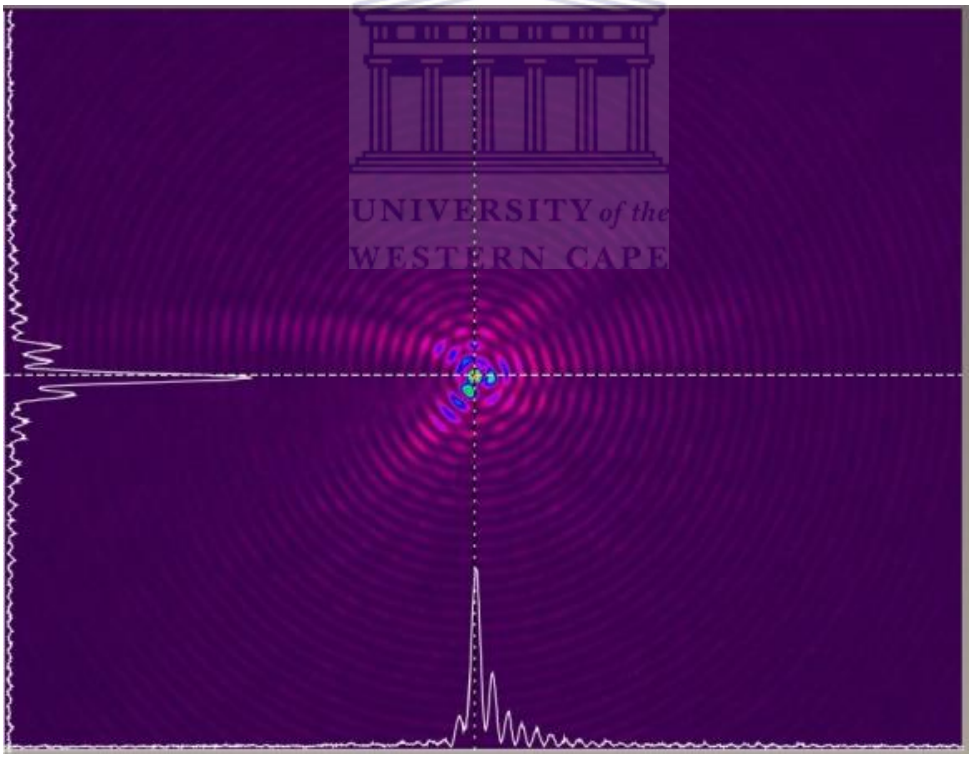

(b)

Figure 2.18: Images of the initial Gaussian beam (a) illuminated onto the axicon with its resulting Bessel beam (b).

UNIVERSITY of the
WESTERN CAPE

The same axicon ($\gamma = 5^{\circ}$) was used as in the previous experiments; however since the operating wavelength and the beam width differs from those of the previous laser, different results were expected. The central spot size is smaller, whereas the propagation distance is longer than that of the fibre laser. The beam diameter was measured along the Bessel beam propagation region and as observed in Fig. 2.19, the diameter retains almost the same size in that region. The calculated value for the central spot diameter was 13.56 µm, whilst the diameter was measured to be 12.8 µm ± 0.3 µm.

The calculated value of the propagation distance for the femtosecond laser was found to be $z_{max} = 55.46$ mm thus $\frac{1}{2} z_{max} = 27.73$ mm. The measured value for half the propagation distance was verified by measuring the peak intensity counts along the Bessel beam propagation region. As seen in Fig. 2.20 the peak intensity increases with increase in propagation distance, it then becomes constant from 22 mm till about 26 mm, thereafter it drops down. The $\frac{1}{2} z_{max}$ value was averaged to be 24.0 mm which corresponded well to the calculated value of 27.73 mm.

UNIVERSITY of the
WESTERN CAPE

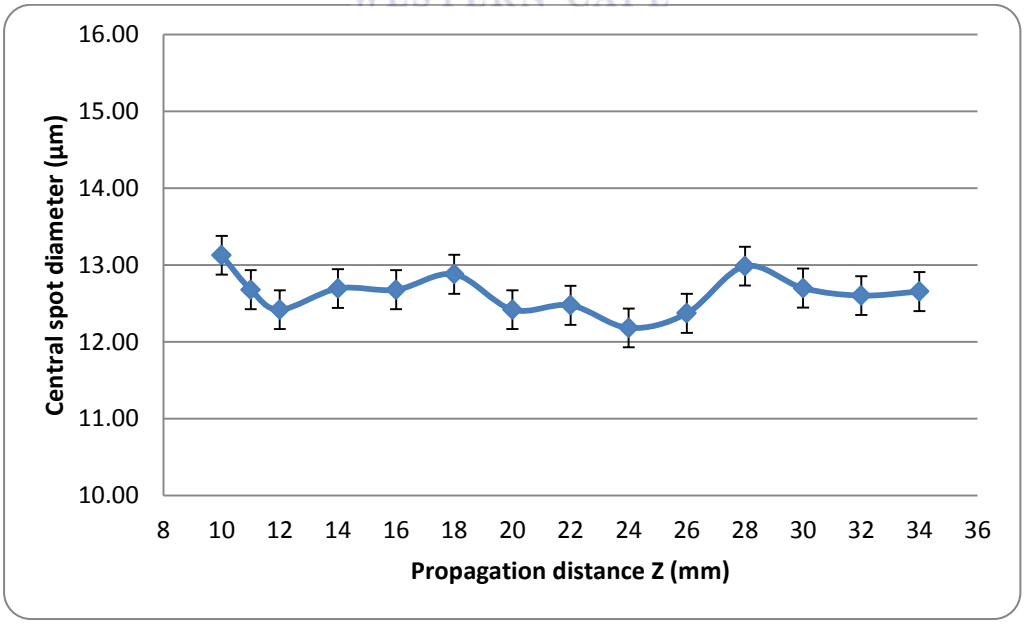

Figure 2.19: A graph illustrating the diameter of a central spot of a Bessel beam generated using a Ti:Sapphire femtosecond laser.

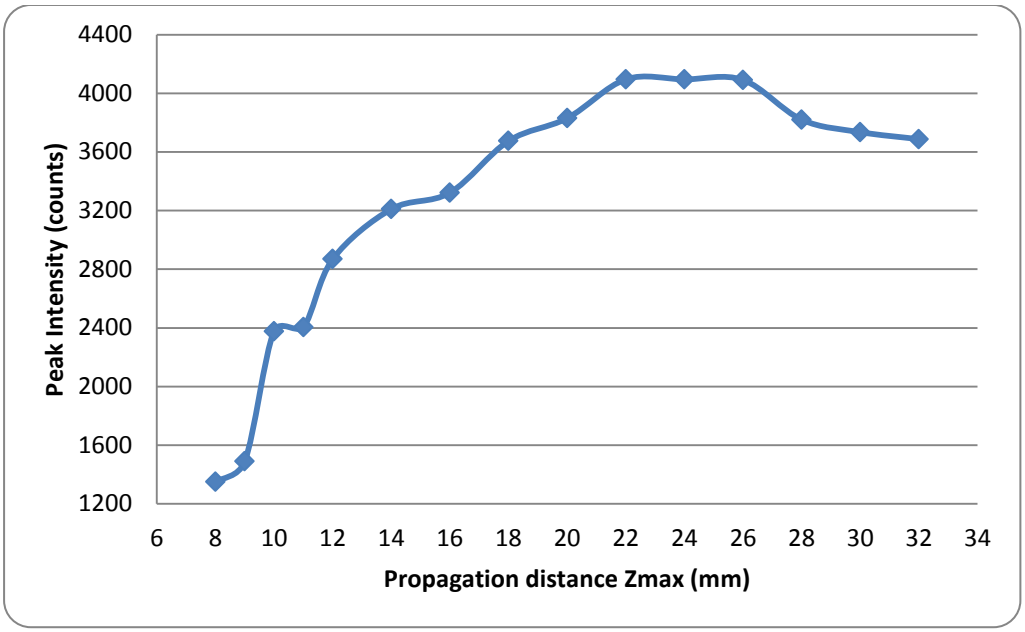

Figure 2.20: A graph illustrating the peak intensity profile along the propagation distance for a Bessel beam generated using the Ti:Sapphire laser.

UNIVERSITY of the
WESTERN CAPE

The diameter of the annular ring depends entirely on the focal length of a particular lens, whereas the thickness of the ring depends on the beam width. In order to vary the diameter of the annular beam, two lenses of different focal length were used. It can be seen in Fig. 2.21 that a lens with a short focal length results in a smaller ring diameter as compared to a lens with a longer focal length. The diameter increases with an increase in length *L* as shown in Fig. 2.9 however maintaining the same ring thickness *t*. The diameter of the annular beam generated using a lens with focal length $f = 60$ mm was measured to be 3.2 mm ± 0.5 mm and that for the lens with focal length $f = 100$ mm lens was measured to be 5.1 mm ± 0.5 mm. The intensity of the annular beam is not evenly distributed; this is caused by the initial beam shape since it is not entirely circular.

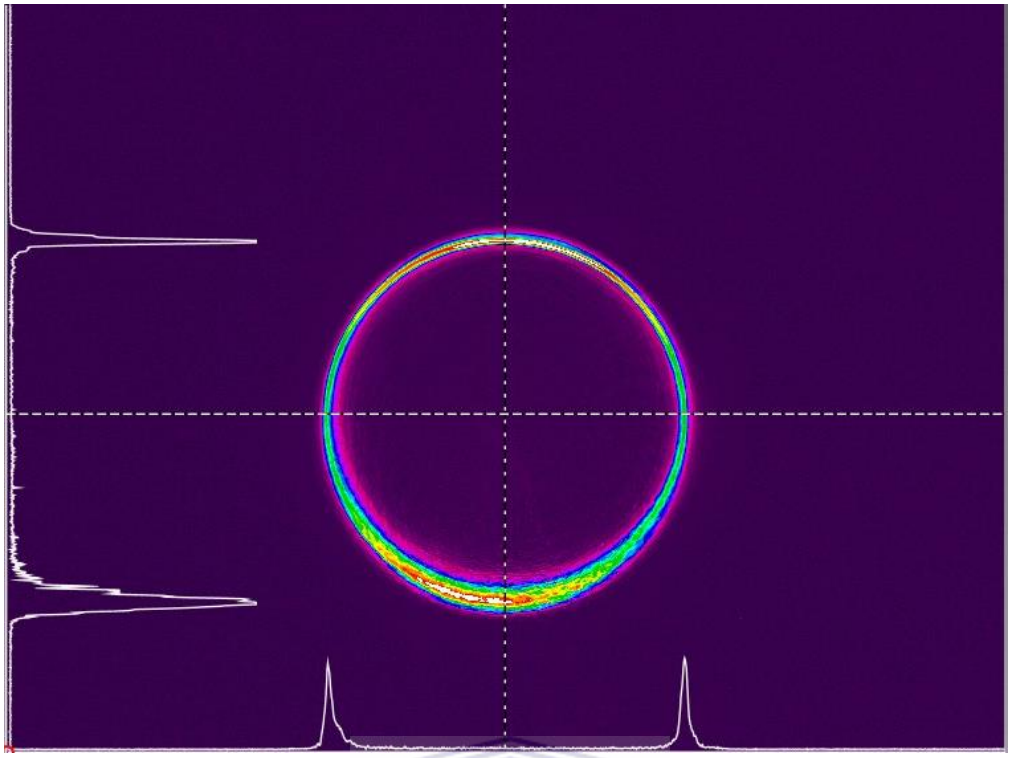

(a)

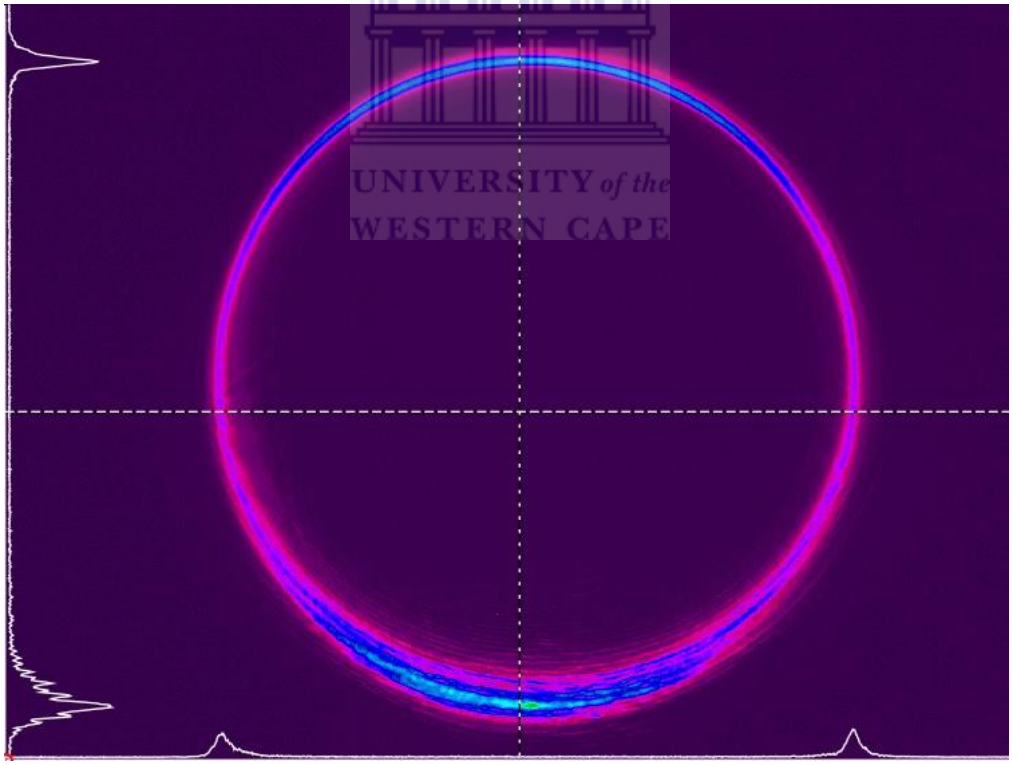

(b)

Figure 2.21: Annular beams generated using lenses of different focal length, (a) 60 mm focal length lens, and (b) 100 mm focal length lens.

UNIVERSITY of the
WESTERN CAPE

2.6 Conclusion

In this chapter laser beam shaping was discussed with the main focus on Bessel beams. Zero order Bessel beams theory was discussed and ways to generate these beams were also discussed. These beams are known to possess a large focal depth as compared to Gaussian beams, this was proved experimentally when the propagation distance was measured and the beam maintained the same central spot size along the Bessel beam propagation region.

The ability of Bessel beams to reconstruct after encountering an obstacle and its large focal depth has prompted interest in using these beams for different applications in material processing industries. Laser drilling is one of the machining processes with applications in different industries. Laser drilling on different materials with Bessel beams was investigated; the results are presented and discussed in the next chapter.

UNIVERSITY of the
WESTERN CAPE

Chapter 3
Laser drilling

3.1 Introduction

Over the years lasers have gained popularity in machining of different materials in various industries such as aviation and automotive amongst others. The reason for such popularity is mainly because lasers perform fast and precise machining. The process of laser machining involves removal of material from a workpiece through laser interaction [3-5, 33]. During this interaction photon electromagnetic energy is transported into the target material, where it is converted into thermal energy. The material is removed from the target either by melting, a combination of melting and vaporization and/or ablation. In the absence of vaporization and ablation molten material is removed by the mechanical force of an assist gas jet. Laser machining processes includes amongst others, laser drilling, laser cutting, laser welding, and marking or scribing [34]. In this dissertation the focus is on laser drilling and its applications.

UNIVERSITY of the
WESTERN CAPE

Laser drilling is one of the oldest laser machining processes with applications in the automotive industries, medical engineering fields, electronics industry, and aviation industries [3-5]. It is a noncontact, precise, and reproducible technique that is used to form small diameter (≤ 100 μm) and high aspect ratio holes in a wide range of materials [5]. It is considered as an alternative for drilling techniques such as mechanical drilling, electro discharge machining, electrochemical machining, and electron beam drilling, for holes with diameters less than 0.25 mm [3-5]. Laser drilling has the ability to drill holes as small as 10 μm in difficult-to-machine materials such superalloys, ceramics, and composites without tool wear [5].

Holes as small as 1 μm can be drilled using the ultrashort pulsed lasers. Hole size is best defined in terms of the aspect ratio (a ratio of hole depth to diameter at the midspan of the hole). For a particular material the limiting aspect ratio depends on both the optical characteristics of the laser beam and the thermo-physical properties of the material [35].

For drilling to take place, a high intensity beam is focused onto the surface at high power densities ($\geq 10^7$ W/cm^2) [2, 35] sufficient to heat, melt and subsequently eject the material in both liquid and vapour phases [5]. Drilling is mostly carried out with a pulsed laser, where the pulse duration is significantly shorter than the thermal response time of the material. There are four most popular techniques used for laser drilling processes and these techniques are discussed in the following sub-section.

3.1.1 Laser drilling techniques

Depending on the requirements concerning geometrical characteristics (diameter, depth, taper and aspect ratio), quality (precision), and productivity (drilling time); four different drilling techniques are commonly used i.e. single pulse drilling, percussion drilling, trepanning, and helical drilling [3-5]. Schematic diagrams of drilling techniques are illustrated in Fig. 3.1.

Single-pulse drilling (Fig. 3.1 (a)) with laser radiation is regarded as the most productive of all the above mentioned techniques. It operates with pulse durations in the range of microseconds to milliseconds, also with the ability to reach a drilling depth of up to 2 mm. It is used in applications that require a large number of holes with diameters $\leq$ 1 mm and depths $\leq$ 3 mm [3-5,35].

Percussion drilling (Fig. 3.1 (b)) is a pulsed process, in which material is removed with consecutive pulses of laser radiation [35-36]. It is applied for holes with diameters $\leq$ 1mm and depths up to 20 mm. Through this technique a high aspect

ratio can be achieved as compared to the single-pulse drilling method (approximately 50:1 compared to 20:1). Pulse durations for this technique range from about 100 fs to 2 ms and the diameters ranges between 100 μm and 1 mm [3-5]. Pulsed Nd:YAG lasers are commonly used for percussion drilling because of their higher energy per pulse and high peak power. One disadvantage of percussion drilling is that the material which is removed is blown backward toward the lens. Applications of this technique include the drilling of cooling holes in the turbine blades of aircraft engines and stationary turbines, holes in filters, sieves, nozzles for ink-jet printers, and feed-through holes for solar cells [3].

Trepanning (Fig. 3.1 (c)) is a combination of the cutting and drilling processes, typically performed using a pulsed laser. The pulse duration selection (ranging from a few nanoseconds to millisecond) is dependent on the type of material, the thickness of the material and the required quality of the hole. A through hole is first pierced by percussion drilling and then the through hole is widened to its final diameter in a circular cutting motion. The required diameter can be achieved either directly in a single positioning step or in several consecutive positioning steps with the beam describing concentric circles or spirals [3].

UNIVERSITY of the
WESTERN CAPE

The helical drilling technique (Fig. 3.1 (d)) requires rotation of the laser beam relative to the workpiece or vice versa. Unlike trepanning helical drilling does not involve the creation of a pilot hole. The laser moves in circles over the material as the pulses are delivered and a large amount of material shoots up during the process. The laser continues to work its way through the hole in a downward spiral. The drilling process is dominated by vaporization which helps to avoid the formation of a large melt pool at the hole bottom. The pulse duration for this process is in the nanosecond range. Helical drilling has the ability to produce large and deep high-quality holes that are very precise and exhibit good micro-structural quality [3].

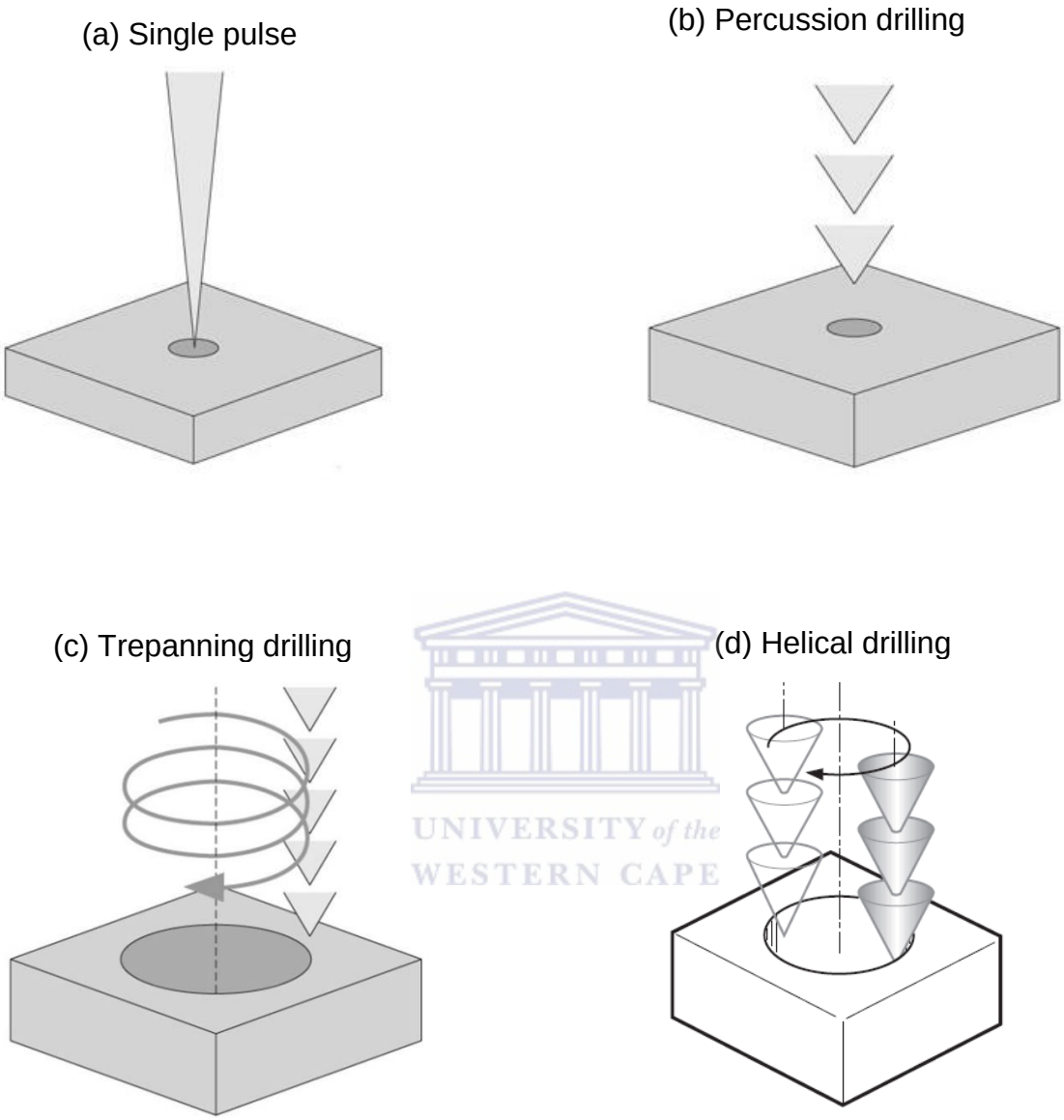

UNIVERSITY of the
WESTERN CAPE

Figure 3.1: Laser drilling techniques (a) single pulse drilling, (b) percussion drilling, (c) trepanning drilling, and (d) helical drilling [3].

For this dissertation the percussion drilling technique will be considered. The Ti:Sapphire femtosecond laser can perform percussion drilling in two ways, i.e. burst mode and continuous pulsed mode.

3.1.2 Defects associated with laser drilling

The principal characteristics of laser drilling processes include the hole diameter, depth and drilling angle. Like any other machining process, laser drilling also suffers from defects. The common process defects associated with laser drilling are tapering of the hole walls, recast layer, spatter, and microcracking [6, 35-38].

In contrast to mechanically drilled holes, laser drilled holes are not entirely parallel walled and in most cases they are associated with taper. Tapering refers to the decrease of the hole diameter with depth. The taper in laser drilled holes is caused by the expulsion of molten and vaporized material from the hole, and is defined as:

$$\varphi = \frac{d_i - d_j}{2t}, \qquad (3.1)$$

where φ is the taper angle, d_i and d_j are the entrance and exit diameters respectively, and t is the thickness of the material [5]. Figure 3.2 is a schematic description of the side view of the hole taper.

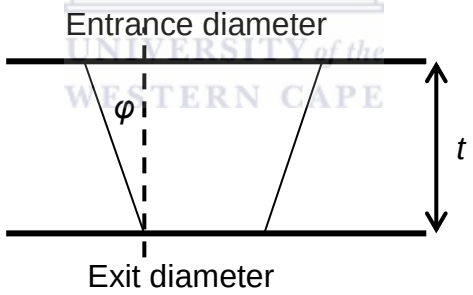

Figure 3.2: Schematic diagram illustrating the description of the hole taper.

The recast layer is classified as resolidified material that remains on the sides of the wall of the drilled hole. Some of this resolidified material is found at the entrance and exit surface of the hole. When the resolidified material is on the entrance surface it is called spatter and when it appears on the exit surface it is referred to as dross [34]. The resolidified layer can generate micro-cracks that can propagate into the parent material [35-38]. Microcracking arises when drilling brittle or high hardenability materials, and often results from high cooling rates caused by high temperature gradients.

3.1.3 Laser Parameters that affect laser hole drilling process

The laser drilling process is mostly influenced by pulse energy density, pulse duration, number or pulses, laser wavelength and beam quality. Previous work has revealed that optimizing laser parameters including average power, pulse frequency, and focal position can minimize the defects [36] discussed in subsection 3.1.2 and improve the hole quality.

3.1.3.1 Pulse energy

The pulse energy is described as the total optical energy content of a pulse, i.e. the integral of the pulse's optical power over time. It is calculated by dividing the average power (which can be measured by a powermeter) by the pulse repetition rate. The pulse energy and pulse duration are often used to determine the peak power of a pulse [39].

UNIVERSITY of the
WESTERN CAPE

Depending on the type of laser, the pulse energy can range from picojoules to kilojoules, for example Q-switched laser have pulse energies ranging from microjoules to milijoules, while mode-locked lasers have low pulse energies ranging from picojoules to nanojoules or microjoules [39]. Holes drilled with high pulse energy lasers have large diameters and large hole-depth. The high pulse energy causes the exit diameter to increase due to pressure exerted by the vaporization of the material in the hole [6]. Baricholo et al. [40] attested to this by setting all other parameters constant and only varying the pulse energy.

3.1.3.2 Peak power

The peak power of an optical pulse is defined as the maximum optical power. Whilst the peak power density is the power per unit area usually expressed in terms of W/cm^2. For a beam with a small unit area, the peak power density is very high. Lasers with ultrashort pulse durations also result in higher peak powers to the order

of gigawatts [39, 41]. Peak power for lasers with long pulses can be measured using a photodiode which monitors the optical power versus time. This method is not compatible with lasers that have pulse durations that are below a few tens of picoseconds, instead the peak power for such lasers is calculated from the pulse energy and pulse duration.

As the peak power increases the hole's exit diameter becomes larger than the entrance diameter, this is known as negative taper [37]. The average taper angles decrease with the increasing peak power. This is because higher peak powers leads to more vaporization and ablation and less melting. Thus more material is removed from effectively at the bottom of the hole resulting in large exit diameters.

3.1.3.3 Number of pulses

Increasing the number of pulses increases the depth of hole, until certain number of pulses is reached, thereafter the depth remains constant because the material can no longer escape from the hole. [37]. This can be illustrated by the percussion drilling technique, since it involves laser pulses being delivered successively at the same spot. Each pulse removes some material. The disadvantage of the percussion drilling technique is that as the number of pulses increase, the recast from the drill hole accumulates until the melt forms a closure.

As the depth of the hole increases, the pressure required to blow out the molten material increases also [5]. At the closure, the laser radiation is reflected, diffracted and absorbed and the solidified mass is re-melted. This process recurs at different points in the drill hole due to consecutive pulses. The absorption of the laser radiation at a closure by solidified melt can results in local expansion of the drill hole and thus a reduced reproducibility of the drill hole geometry [3]. As the number of pulses increases the diameter of the drilled hole increases and becomes more circular.

UNIVERSITY of the
WESTERN CAPE

3.1.3.4 Pulse duration and frequency

The pulse duration and pulse shape have a huge impact on the quality of the drilled holes [42]. Kacar et al. [37] showed that the average hole diameters increased with increasing laser pulse duration. They also showed that the average taper angles decrease with increasing pulse duration, resulting with a negative average taper angle. The use of extremely short nano-, pico-, and even femtosecond pulse durations minimizes the thermal effects such as melting and recast layer. Micro-cracking at the side-walls of the laser drilled hole is reduced when using pulses in these ranges and the need for any post processing measures are reduced when using pulses in these ranges.

Bandyopadhyay et al. [6] noted that the taper angle reduces with increasing pulse frequency regardless of the material-thickness. They also found out that the pulse frequency has a significant bearing on the number of pulses required to drill a through hole. A Ti-6Al-4V material of thickness 8 mm was drilled through in 25 pulses at a frequency of 9 Hz whereas at 6 Hz twice the numbers of pulses were required.

UNIVERSITY of the
WESTERN CAPE

3.1.3.5 Focusing conditions

Various optical instruments are used to determine the focal length, depth of focus and focal spot size of the beam. The spot size of a focused laser beam determines the size of the drilled holes on the specimen. The minimum spot diameter depends on the focal length of the lens used, beam quality, laser wavelength, diameter of the laser beam, and the geometry of the lens. In the case of Bessel beams the opening angle of the axicon is influential on the central spot size, if γ is small, then r_0 is large and vice versa [1].

The point of focus is very crucial when drilling especially with the Gaussian mode. The specimen surface has to be placed exactly at the focal range of the beam, placing it before or after leads to poor results. Baricholo et al [40] discussed

the importance of placing the specimen at exactly the focal point. However this is not the case for Bessel beams and optical arrangements with a large depth of field i.e. good beam quality and long focal ranges. Bessel beams have a longer focal depth, thus the specimen can be placed anywhere in the Bessel beam zone.

3.1.3.6 Assist gas

Most of the laser drilling processes use an assist gas jet coaxial to the laser beam. The pressure from the assist-gas has an effect on the quality of the hole, as the assist gas is used as an aid to the removal of plasma and debris and also prevents contamination of the focusing optics by the ejected debris. The type of gas used and the operating pressure at which it is applied play a very important role in laser drilling. At high power lasers, wherein vaporization takes place, the assist gas increases the drilling efficiency by removing the absorptive vapours and debris that can prevent the incident laser energy from reaching the target. The most used assist gases are oxygen, argon, nitrogen and compressed air. Inert gases are used when oxide free holes are desired, whilst oxygen is mostly used to enhance the material removal by exothermic reaction [3,5].

UNIVERSITY of the
WESTERN CAPE

3.2 Ultra-short pulsed lasers

With high demand in miniaturization of good quality holes in industries, much focus has been shifted to micromachining materials using ultrashort lasers. The reason for this move is mainly because ultrashort lasers have large broadband optical spectrum and high peak intensities that allows micro- and nano-structuring of all materials [27]. Another major reason for the use of ultrashort pulse lasers is their ability to achieve a thermal material removal. They possess very high power densities such that the melting and thermal conditions are completely eliminated and the material removal occurs only through ablation. Ultrashort pulses have pulse duration in the order of femtosecond (10^{-15} second) or less. The most common of these ultrashort lasers are

the femtosecond lasers which are described as lasers that emit optical pulse with duration between a few femtoseconds and hundreds of femtoseconds [39].

The key performance parameters of these lasers are: pulse duration, pulse repetition rate, pulse energy and the average output power. There are different types of femtosecond lasers with the most common ones being solid-state lasers, fiber lasers, dye lasers and semiconductors.

Femtosecond pulses have been shown to produce damage-free micromachining in a wide range of materials [42-45]. The femtosecond pulses offer advantages over the long pulses due to its ability to deposit the energy onto a material in a very short time before thermal diffusion can occur. This results in reduction of the heat-affected zones, minimal or no recast layers, and high aspect ratios. Bhuyan et al. [27] used high-aspect ratio Bessel beam to overcome the difficulties associated with femtosecond micromachining using Gaussian beams in fabrication of glass microchannels. The advantages of using Bessel beams are further discussed in the following subsections. Femtosecond Bessel beam machining has been investigated for laser processing of metals [1], laser surface nanoprocessing [44] and index modification in glass [27].

UNIVERSITY of the
WESTERN CAPE

3.3 Applications of Bessel beams in micro-drilling

3.3.1 Literature review

Most laser drilling processes are conducted using Gaussian beams, mainly because the Fourier transform remains a Gaussian thus preserving its shape as it passes through optical systems. In material processing the preservation of the beam shape is crucial as the beam travels through different optical mediums to the specimen. It is mentioned in chapter 2 that most lasers operate in fundamental transverse electromagnetic mode of a cavity providing a Gaussian intensity profile. However there are some deficiencies associated with Gaussian intensity profile beams that

have prompted the use of different beam shapes in material processing. Non-conventional beams such as Flat-top beams and Bessel beams are amongst those that have been considered for material processing [7]. In this dissertation the use of Bessel beams in material processing in particular laser drilling is considered.

Non-conventional beams have the advantage that they can be explicitly designed to meet the requirements of a given material configuration or application that could not be feasible with Gaussian beams. As discussed in chapter 2, a Gaussian beam has a short focal depth as compared to that of a Bessel beam. For laser micro-drilling focusing a laser beam tightly on the material is very important. This can be achieved by focusing a laser beam with a conventional convex lens to its waist diameter [7]. The disadvantage to this setup is that the focal depth is so short, meaning that the beam is approximately parallel only over a very short distance. The beam outside the Rayleigh range is either converging or diverging (see Fig. 2.1) and this is not ideal for drilling deep holes without taper. Due to the beam divergence the specimen has to be placed exactly within the Rayleigh range. This becomes a challenge when drilling uneven, rough substrates or non-planar substrates. Thus a beam with a small diameter that does not depend on propagation length becomes very useful in applications of microdrilling. Bessel beams do not face such challenges as they are parallel over a much longer distance.

UNIVERSITY of the
WESTERN CAPE

When drilling rough or uneven specimens using conventional beams, a high numerical aperture lens would be required to create a tight focus, thus producing a short depth of field. In order to obtain holes of the same size on surfaces at different heights, the position of the beam must be adapted to the specimen's irregularities in order to preserve the working distance. Bessel beams were considered as an alternative solution to this problem because of their special property mentioned above. The long depth of field helps with increasing the tolerance of the focal plane during processing and also prevents optics being contaminated with the debris coming from the processed sample.

Kohno and Matsuoka [2] verified the case that Bessel beams have longer focal depth, when they changed the work distance within a range of several millimetres and still maintain the diameter of the laser fabricated spots on a silicon wafer to approximately 1 μm. Courvoisier et al. [44] used the same approach when writing 500 nm diameter nano-craters over a longitudinal positioning range exceeding 20 μm.

The depth and diameter of the hole drilled when using Bessel beams are dependent on the opening angle of the axicon. A small focal spot diameter and a short propagation distance are obtained using a Bessel beam with a large opening angle *θ.* Matsuoka et al. [1] varied the focal spot and focal depth by changing the opening angles of axicons. They showed results for three axicons (with base angles $\gamma = 10°$, $5°$ and $1°$). The axicon with the smallest base angle i.e. $\gamma = 1°$ resulted in a large spot diameter (37 μm), and deep focal depth (≈ 20 mm), as compared to the results obtained when an axicon with a large base angle $\gamma = 10$ (spot diameter 3.6 μm and focal depth 0.7 mm) [1] was used.

To drill holes with deep focal depth, an axicon with a small opening angle *θ* can be used. The drilled hole's diameter is expected to be a little bit larger than the focal spot diameter when drilling using Bessel beams because the energy density of the Bessel beam's surrounding rings exceeds the processing threshold.

It has been numerically demonstrated that the penetration depth of Bessel beams propagation inside a hole in bulk material is substantially longer than the penetration depth achievable by a conventional Gaussian beam of the comparable transverse dimensions [22]. This effect was observed for different type of materials such metals, semiconductors, and glass. Upon drilling of copper foil of thickness 100 μm, Alexeev et al. [22] observed that the exit hole deviates from being circular. Also noted was that the diameter of the entrance hole is slightly larger than the expected diameter, due to the high intensity of the first few surrounding rings.

UNIVERSITY of the
WESTERN CAPE

Although the use of Bessel beams in material processing has generated interest from researchers, two major disadvantages of these beams has led to the questioning of the effectiveness of drilling through holes on metals. Bessel beams carry the same amount of energy in their rings with only the intensity differing per ring. The energy in the rings causes the top surface of the material to be ablated and only the central lobe making a hole. This resulting concentric ring structure on the substrate surface around the central hole is undesired in any material processing application. Kohno and Matsuoka [2] suggested that by controlling the beam energy strength only for the main lobe of the Bessel beam to exceed the ablation threshold, the ring structure can be minimized.

The second aspect that limits the use of Bessel beams for through-hole drilling in metals is the inability of the beam to reconstruct itself as the metal surface blocks the rings from the beam itself. As mentioned before (section 2.3) Bessel beams are able to reconstruct a certain distance after encountering an obstacle, since they are a result of the interference between plane waves. Since metals are opaque such plane waves do not propagate inside the material, thus losing the long depth of field of a Bessel beam. However if the drilled metal foils are thin enough (≤ 100 μm), holes drilled with Bessel beams can exhibit sharper sidewalls and produce holes with little taper.

UNIVERSITY of the
WESTERN CAPE

3.3.2 Experimental procedure

A large portion of this dissertation consisted of generating Bessel beams and measuring their properties. Chapter 2 gives a clear description on the generation and the properties of Bessel beams. These beams are then applied in laser microdrilling of stainless steel plates of different thicknesses. The femtosecond machining source used in this work was a Ti:Sapphire amplifier laser (Clark-MXR CPA series) operated at a centre wavelength of 775 nm, pulse duration of $\tau = 150$ fs (FWHM), average power of 1.1 W, and pulse repetition rate 1 kHz. The laser was chosen because of it suitability in drilling processes, mainly because it is pulsed, consists of ultra-short pulse duration reducing the interaction time with the sample, possesses a good

beam quality suitable to generate a Bessel beam, and its ability to reach high peak powers.

Figure 3.3 is a schematic diagram for the experimental setup. The mirrors are used to guide the beam along its optical path. An assist gas (argon) is co-aligned with the incoming laser beam towards the sample. This is to assist in blowing away the debris from the optical elements in the setup and to shield the interaction zone from the atmosphere in order to avoid oxidation.

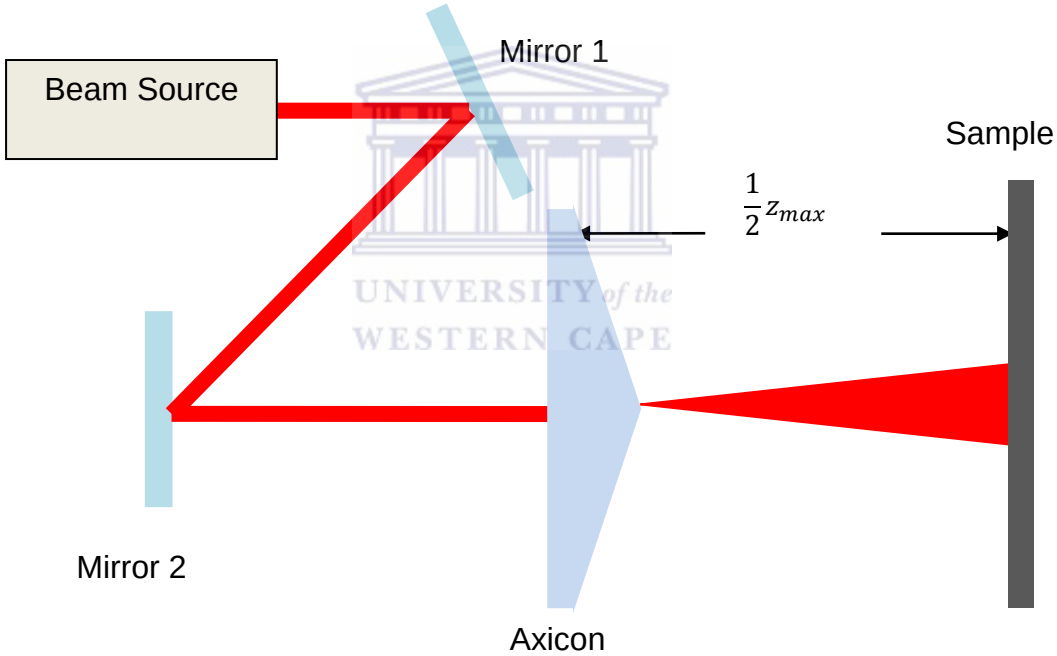

Figure 3.3: A schematic diagram of the experimental setup for laser drilling using Bessel beams.

The incoming Gaussian beam as seen in Fig. 3.4, with a beam width $\omega_0 = 2.55$ mm, and beam quality $M^2 = 1.4$ was illuminated on an axicon with a base angle $\gamma = 2.2°$ to generate zero order Bessel beams.

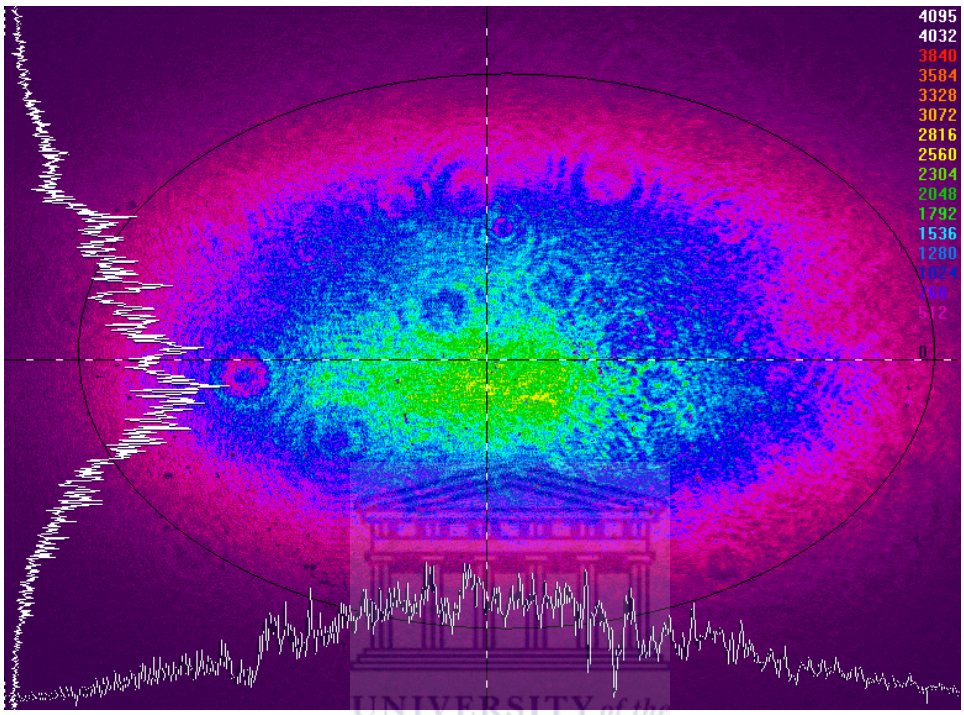

UNIVERSITY of the
WESTERN CAPE

Figure 3.4: An image of the Gaussian beam profile obtained from the Clark-MXR CPA series Ti:Sapphire femtosecond laser.

3.4 Characterisation techniques

For the analysis and measurements of the hole diameter two characterisation instruments where considered, i.e. the optical microscope and the scanning electron microscope. An optical microscope is used to measure the dimensions on the holes, whereas a scanning electron microscope (SEM) is used to view in more details the morphology and topography of the drilled holes up to nanometre scale and measure their diameters.

3.4.1 Optical Microscopy

An optical microscope (OM) is commonly referred to as a light microscope, it uses visible light and a system of lenses to magnify images of small samples. In generating micrographs using the light microscope, a normal light-sensitive camera can be used to capture images.

Two basic configurations of the conventional optical microscope exist, i.e. the simple (single lens) and the compound (many lenses). Most research microscopes are compound microscopes. In order to focus at different focal depths the distance between the sample and the lens is adjusted, whilst a different magnification objective lens can be used to get a wider or narrower field.

A single microscope uses only one lens for magnification, whilst the compound microscope uses multiple lenses to collect light from the sample and a separate set of lenses to focus the light into the eye or camera. Although compound microscopes are more expensive than simple microscopes they have an improved numerical aperture, reduced chromatic aberration and exchangeable objective lenses that adjust the magnification [46].

UNIVERSITY of the
WESTERN CAPE

The structural components of the light path are mostly common for modern optical microscopes. The most common components as shown in Fig. 3.5 are eyepiece (ocular lens), objective turret, and objective lenses, focus knobs to move the stage (coarse and fine adjustment), stage to hold the specimen, light source, diaphragm and condenser, and mechanical stage.

Figure 3.5: A typical Optical Microscope with indications of components that make the optical path [47].

The ocular lens's function is to bring the image into focus for the eye and the objective lenses collect light from the sample. There are usually three or more objective lenses that are attached to the turret. These lenses are parfocal meaning that when one changes from one lens to the other, the sample stays in focus. Light microscopes are characterized by magnifications ranging from 5X to 1000X and numerical apertures ranging from 0.14 to 0.7 [46].

3.4.2 Scanning Electron Microscopy

3.4.2.1 Introduction

A scanning electron microscope, (SEM) is a type of microscope that produces images of a sample by scanning it with a focussed beam of electrons. The distinguishing factor between the OM and the SEM lies in the beam sources used, light for OM and electrons for SEM, and in the magnification system. In OM glass lenses are used to magnify the objects, whilst magnets are used in the SEM to bend the beam of electrons for image magnification. The electrons are thermionically emitted from a cathode or a field-emitter, within an electron gun that is situated at the top of its electron-optical column. The emitted electrons form an electron cloud and are accelerated by a set voltage, the electron cloud is then focussed by electromagnetic lenses, coils and apertures into a fine probe that systematically scans over the specimen surface, to produce an image [48]. The components that make the electron-optical column of the SEM mentioned above are shown in the schematic diagram given by Fig. 3.6.

UNIVERSITY of the
WESTERN CAPE

Two condenser lenses situated below the electron gun focuses the emerging beam into a much smaller diameter size. The beam is further aligned and focused by apertures and coils within the column until it reaches the final lens near the specimen chamber. The fine beam of electrons is scanned across the specimen by the scan coils, while a detector counts the number of low energy secondary electrons. The objective lens determines the intensity of the beam upon striking the specimen and also controls the image brightness.

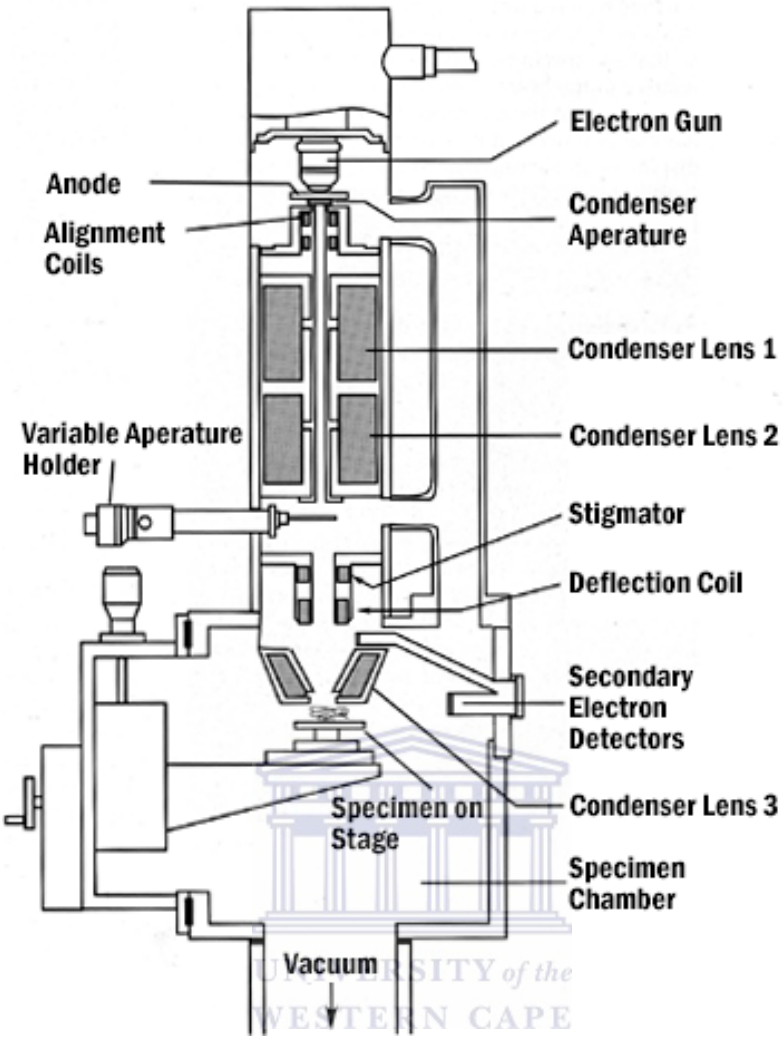

Figure 3.6: Schematic representation of the components comprising the SEM column [49].

3.4.2.2 Electron Beam - Specimen Interaction

When incident electrons are decelerated in the solid specimen, a variety of signals are produced by the electron-specimen interaction. These signals include secondary electrons, backscattered electrons (BSE) and diffracted backscattered electrons, visible light (cathodoluminescent), characteristic X-rays, and Auger electrons. The signals that can be detected in an electron microscope are shown in Fig. 3.7.

The analysis of these signals provides visual information about the specimen's topography, elemental composition and content, as well as other properties such as electrical conductivity. Secondary electrons are valuable in showing the morphology and topography of the samples, whilst backscattered electrons are most valuable for illustration in composition contrast in multiphase samples [48-51].

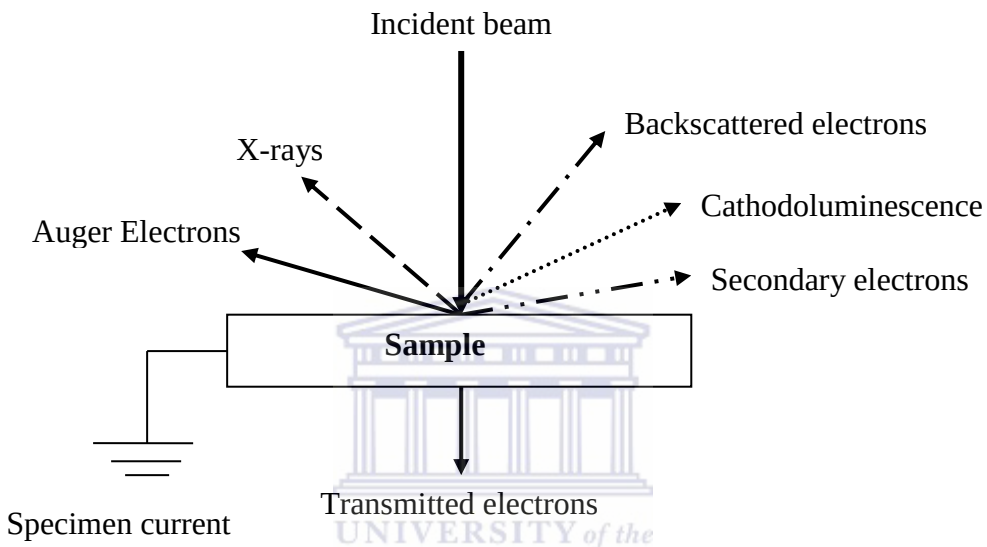

UNIVERSITY of the
WESTERN CAPE

Figure 3.7: Schematic diagram of the signals generated during the incident beam-specimen interaction [51].

Secondary electrons are low-energy electrons that are produced within the interaction volume. The electrons that are produced deeper within the interaction volume are likely to be absorbed through collisions and their energy exhausted before they reach the sample surface. The electrons produced in the near surface reach the secondary electrons' detector and they participate in the formation of the image.

Secondary electrons are produced when an incident electron excites the specimen electron and loses some energy in the process. The excited electron undergoes elastic and inelastic collisions as it moves towards the surface and it will

escape. The electrons that are close to the surface are the only ones with the remaining sufficient kinetic energy to escape.

The secondary electron signal is the most commonly used to image the specimen in modern SEMs. The secondary electron detector captures the electrons, whose energy is then converted into photons by means of a scintillator. The interaction volume is very small when compared to back-scattered electrons or X-rays.

The number of secondary electrons emitted can be maximised by coating a non-conductive specimen with a carbon layer, gold or gold-palladium layer [49, 51]. Areas ranging from approximately 1 mm to 5 µm in width can be imaged in a scanning mode using the SEM, with magnification ranging from 20X up to 30000X.

3.4.2.3 Resolution

The apparatus's resolution is one of the key factors when performing microscopy. Resolution is described as the distance at which two objects are observed as two separate entities. When operating the SEM obtaining great magnifications without sufficient resolution is undesirable, since no valuable information will be extracted from such images. Mathematically, the limit of a resolution, i.e. the smallest separation distance at which two objects are resolved, is described by the Abbe's equation

$$d = \frac{0.612\lambda}{n \sin \alpha}, \qquad (3.2)$$

where d is the limit of resolution, λ is the wavelength of the beam, while n is the refractive index of the viewing medium, and α is the convergence angle [51].

Equation (3.2) shows that in order to achieve the best resolution, smaller wavelengths or high values of n and α are needed. In electron microscopy the resolution is controlled by the accelerating voltage. Thus higher accelerating voltages provide the best resolution.

3.4.2.4 Depth of Field and Working Distance

The depth of field (DOF) is defined as the range of positions for the objects at which human eye cannot detect a change in the sharpness of the image. From geometry the depth of field is given by [51]

$$h = \frac{0.61\lambda}{n \sin\alpha \tan\alpha}. \tag{3.3}$$

It refers to the part of the specimen that appears in focus in the final image. Imaging with electrons offers improvement in both resolution and depth of field because for high energy electrons the microscope is operated with smaller values of α.

The working distance is defined as the distance between the final condenser lens pole piece and the uppermost part of the specimen. The working distance directly influences the depth of field observed for a particular sample [51]. A sample scanned at a long working distance results in a great DOF and a decrease in the aperture angle, whereas the one scanned at a short working distance results in an image with low DOF and is scanned at a wide aperture angle [47-49].

Changing the working distance has an influence in the spherical aberrations of the imaging system; this affects the resolution of the final image. Spherical aberrations arise from the geometry of the electromagnetic lenses. They occur because electrons which are closer to the beam optical axis deflect less than those passing through the periphery of the electron beam. This creates more than one focal point and results in an enlarged, non-focused spot. When the working distance is decreased the spherical aberrations effect become less, this result in a smaller, more focused beam spot and yields a better resolved final image [48].

UNIVERSITY of the
WESTERN CAPE

3.4.2.5 Effect of accelerating voltage

The accelerating voltage is described as the voltage that is applied to the filament. The applied voltage creates a current through the filament thus causing it to emit electrons. Accelerating voltages used in SEM varies between 5 kV and 20 kV. Varying the accelerating voltage has an influence on the electron beam-specimen interaction. For low accelerating voltages, the beam interaction with the specimen is confined in the regions close to the surface. This offers detailed image information of the surface as compared to images obtained at higher accelerating voltages. At these voltages the beam penetrates beneath the specimen surface and signals arising from below the sample surface are imaged. An increase in accelerating voltage decreases the amount of spherical aberrations of the system which then enhances the resolution [49]. Low accelerating voltages are applied on the drilled samples for measuring the hole diameter, and high accelerating voltages are used when viewing the side wall of the holes to determine the tapper angle.

UNIVERSITY of the
WESTERN CAPE

3.4.2.6 Sample preparation

The samples should be of an appropriate size to fit in the specimen chamber. These samples are mounted rigidly on a specimen holder called a specimen stub. In order to obtain an image from a conventional SEM instrument without damaging the specimen specimen using the SEM, the specimen has to be electrically conductive at least at the surface. To avoid the accumulation of electrostatic charges at the surface, the specimens must be electrically grounded. Non-conducting specimens are normally covered with an electrically conductive coating for imaging in order to avoid surface charging. Coating of non-conducting materials reduces the thermal damage caused by the beam to the sample. Stainless steel specimens were used, and since the material is electrically conductive there was no need for conductive coating [47-49].

3.4.3 Characterisation

3.4.3.1 Optical Microscopy Instrumentation

The morphology of the drilled holes on both sides of the samples was imaged using an Olympus BX51M optical microscope using the Olympus SC30 camera to capture the micrographs. At low magnification the micrograph displays the entire irradiated area of the top surface showing all the rings, however difficulties are experienced in viewing the drilled hole from the central lobe of the Bessel beam. The sample is turned around to view the exit hole and the diameters are measured and an average value is given for more circular holes. One of the challenges experienced with the OM is that the resolution at high magnification i.e. at 1000X is poor, resulting in difficulties in measuring the diameter at the top surface of the sample. To resolve this mishap the use of SEM was considered.

UNIVERSITY of the
WESTERN CAPE

3.4.3.2 Scanning Electron Microscopy Instrumentation

High resolution scanning electron microscope was used for imaging. Since stainless steel is conducting, there was no need to coat the samples. Secondary electrons imaging was obtained using a gentle-beam mode with accelerating voltage of 2.0 kV and a working distance of 38.0mm. Micrographs were taken up to 2000X magnification. The results are shown and discussed in the next chapter.

Chapter 4
Results and discussions

4.1 Experimental results and discussions

4.1.1 Bessel beam generation

Bessel beams were generated using the setup discussed in subsection 3.3.2. The main properties of a Bessel beam were calculated and measured. The procedure used for measuring the beam profile in chapter 2 was also used in this subsection. The central spot diameter was measured to be 28.2 µm ± 0.5 µm which was in close agreement with the calculated value of 31.70 µm. The propagation distance at half z_{max} was measured at 65.0 ± 0.5 mm which was in agreement with the calculated value of 66.4 mm ± 0.5 mm. The sample was placed at r_{max} position (see Fig. 2.10) which is a halfway the propagation distance z_{max}, and it's the region where the Bessel beam reaches its highest intensity.

UNIVERSITY of the
WESTERN CAPE

The initial beam emitted by the Ti:Sapphire femtosecond laser had an elliptical shape as shown in Fig. 3.4, with a poor quality Gaussian profile. This had a negative influence on the quality of the Bessel beam generated. An ideal Gaussian beam has a beam quality, $\mathrm{M}^2 \approx 1$, and it can be seen in Fig. 2.2 (b), whereas the beam from the current laser had a beam quality $\mathrm{M}^2 = 1.4$. The central lobe is not entirely separated from the first surrounding ring, and the first ring has an unevenly intensity distribution. This could have been caused by the incoming beam profile, or misalignment of the beam in its optical path.

Figure 4.1(a) & (b) displays the intensity profile distribution of a Bessel beam in 2D and 3D respectively. The central lobe of the Bessel beam has the highest intensity and the first surrounding ring has a slightly higher intensity than the other surrounding rings.

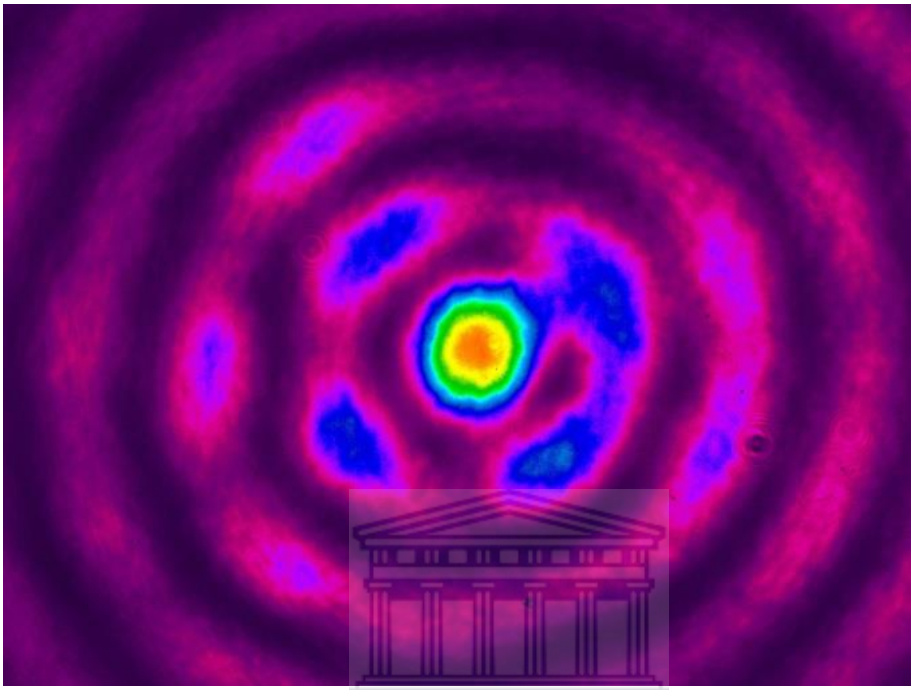

(a)

UNIVERSITY of the
WESTERN CAPE

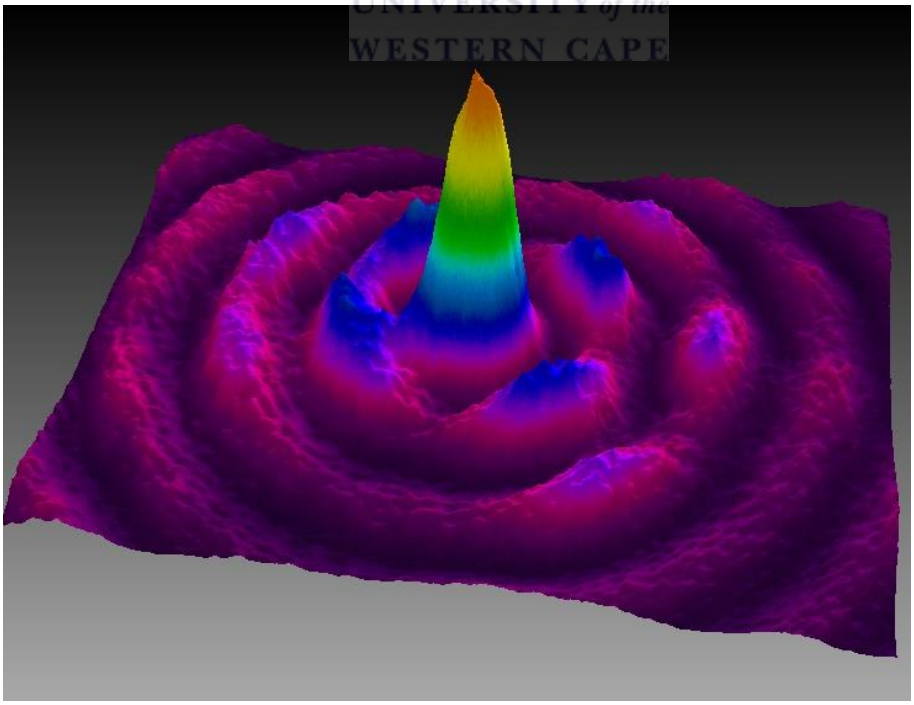

(b)

Figure 4.1: Images displaying intensity distribution in 2D (a) and 3D (b) of a Bessel beam from the Clark-MXR CPA series Ti:Sapphire femtosecond laser.

4.1.2 Laser drilling results and discussions

For drilling, the samples were placed at half z_{max} position as indicated on Fig 3.3, since the central lobe attains its maximum intensity at that position. As discussed in chapter 2 the half z_{max} region is experimentally determined by profiling the beam along its propagation distance and measuring the intensity counts from the BeamGage beam profiler

Stainless steel sheets, 50 µm and 100 µm thickness, were used as samples and they were positioned at half z_{max}. The laser was operated in continous pulses for a period of 30 seconds per sample. The output power measured before the axicon was 0.912 W giving pulse energy of 0.912 mJ. The pulse energy was calculated by dividing the output power with the pulse repetition rate which is 1 kHz for the femtosecond laser used. The energy per ring was calculated to be 14.45 µJ, as stated before the rings in a Bessel beam contain the same amount of energy, with only the intensity changing per ring. Since each ring carries the same amount of energy all visible rings have an interaction with the top surface of the material causing the surface to be ablated. However since the intensity differs, only the rings with high intensity will have more material removed thus the central lobe making a through hole. At 30 seconds a through hole is drilled for both samples, however the beam light can be viewed on a screen, from the exit side of the sample in less than 20 seconds on the 50 µm sample.

To improve on the quality of the hole and also eliminate the debris around the surfaces of the holes, the samples were immersed in a pickling solution. The solution used to clean the samples was a mixture of acids viz. 8-20 vol% HNO3 and 0.5-5 vol% HF. An optical microscope (OM) was used to analyse the morphology of the drilled holes. Figure 4.2 shows micrographs obtained from the OM for stainless steel. Micrograph (a) is taken before the sample is cleaned, and micrograph (b) was taken after the sample was immersed in a pickling solution. The fine features in the region of the through hole could not be resolved with the highest magnification (1000X) of the Olympus BX51M OM microscope. After pickling, the oxides on the top surface of

UNIVERSITY of the
WESTERN CAPE

the material are removed and the depth of the actual material removed can be observed.

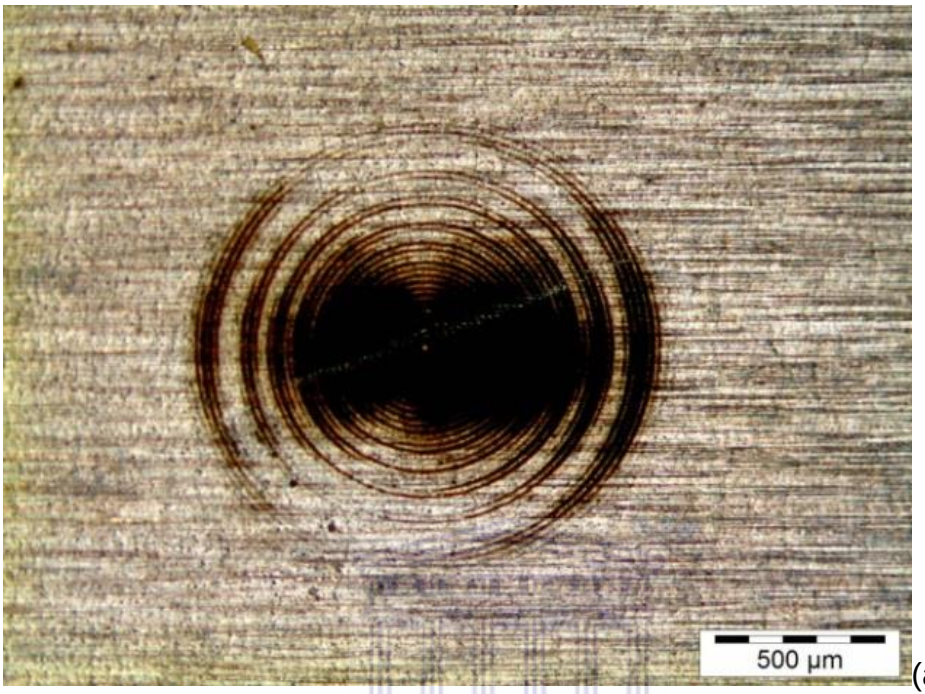

(a)

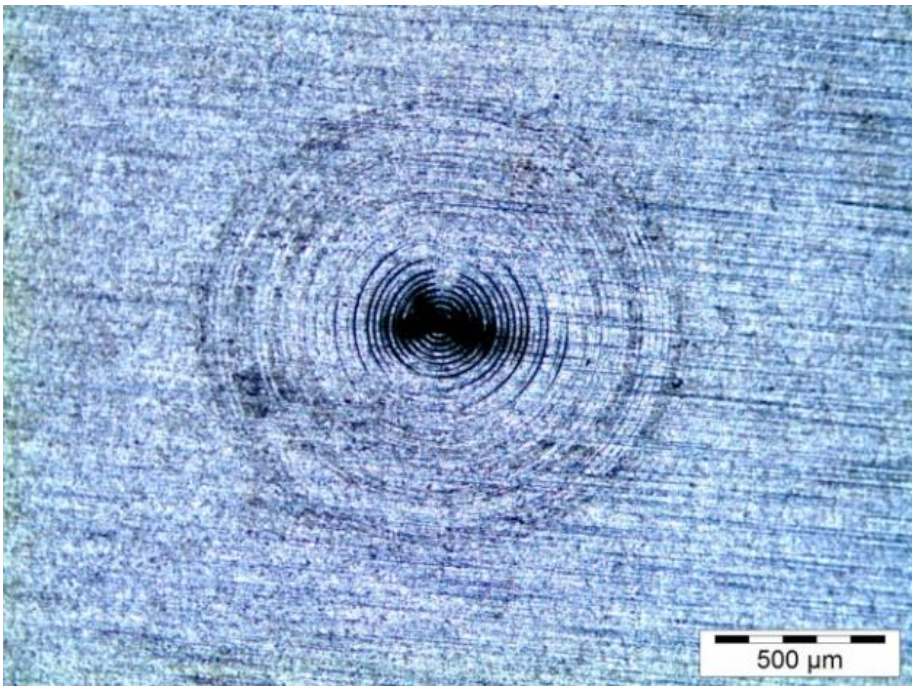

(b)

Figure 4.2: Micrographs of the top surface of laser drilled stainless steel sheets (a) before sample immersed in pickling solution, (b) after the sample is immersed in pickling solution for duration of 30 minutes.

The process gas is used to remove the debris formed on the walls of the drilled holes. Argon serves to block additional chemical reactions from the oxides in the room during the drilling process. There is a difference on the drilled holes morphology when assist gas is used and when it is not. The images in Fig. 4.3 are for 100µm stainless steel sheet drilled with and without the assist gas. The top irradiated surface is ablated by the surrounding rings and the central lobe drills through the material and forms a hole.

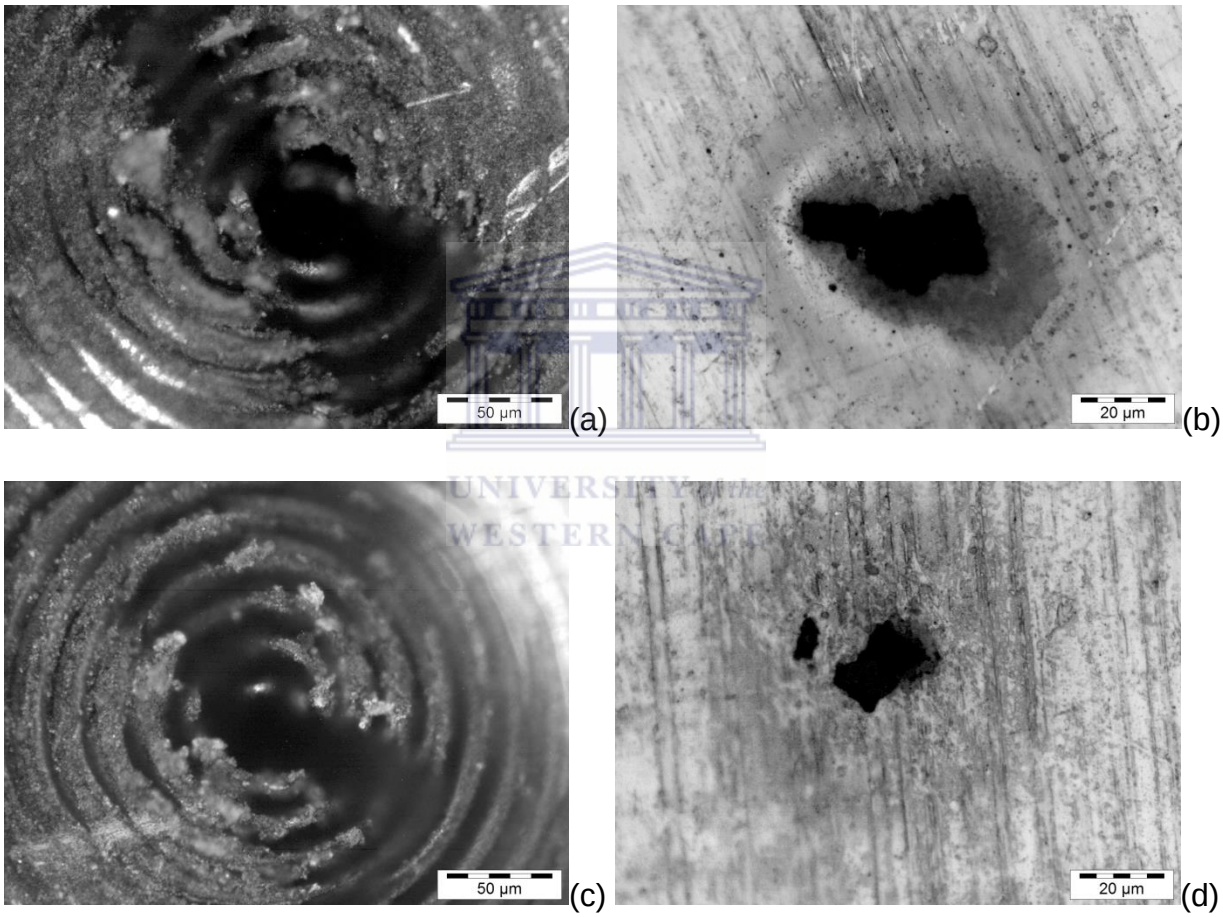

Figure 4.3: Images of laser drilled holes on a 100µm stainless steel sheet. (a) Top surface of the sample and (b) exit hole drilled without the shielding gas. (c) Top surface of the sample and (d) exit hole drilled with a shielding gas, Argon.

UNIVERSITY of the
WESTERN CAPE

The exit hole deviates from being circular as can be seen in Fig. 4.3 (b) and (d). Holes drilled with the assistance of the shielding gas shows less surface oxidation. No phase formation can be observed since ultrafast femtosecond pulses are used for drilling.

Due to poor resolution at high magnification for images obtained using the optical microscope, a SEM was used for imaging the samples at higher magnification. SEM images for drilled samples are shown in Figures 4.4, 4.5 and 4.6. Images obtained before the samples were immersed in an ultrasonic bath contained debris on the edges of the holes as seen in Fig. 4.4 (a) and Fig. 4.5. Although the holes are not circular, they maintain almost the same shape at the top and bottom side of the sample. Debris free holes can be seen in images displayed in Fig. 4.6.

Figures 4.7 and 4.8 displays the entrance and exit diameters of the 50 µm and 100 µm sheets respectively, drilled with the assistance of shielding gas argon. The holes have an elliptical shape, and the diameters were measured at various points in the horizontal dimension. In Fig. 4.7 the vertical diameter was measured to be 63.1 µm, while a number of horizontal measurements were taken with the smallest measurement being 6.42 µm and the largest from the hole being 20.4 µm.

UNIVERSITY of the
WESTERN CAPE

(a)

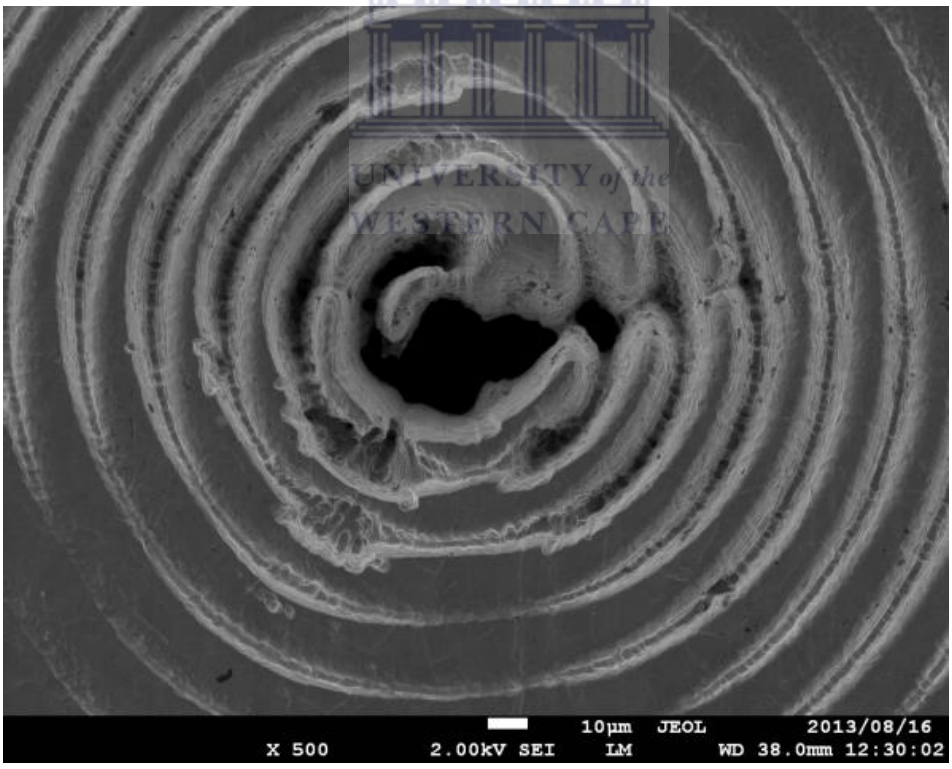

(b)

Figure 4.4: Images of laser drilled holes using a Bessel beam with no assist gas displaying the top surface of a 50 µm stainless steel sheet (a) before ultrasonic bath and (b) after the ultrasonic bath.

UNIVERSITY of the
WESTERN CAPE

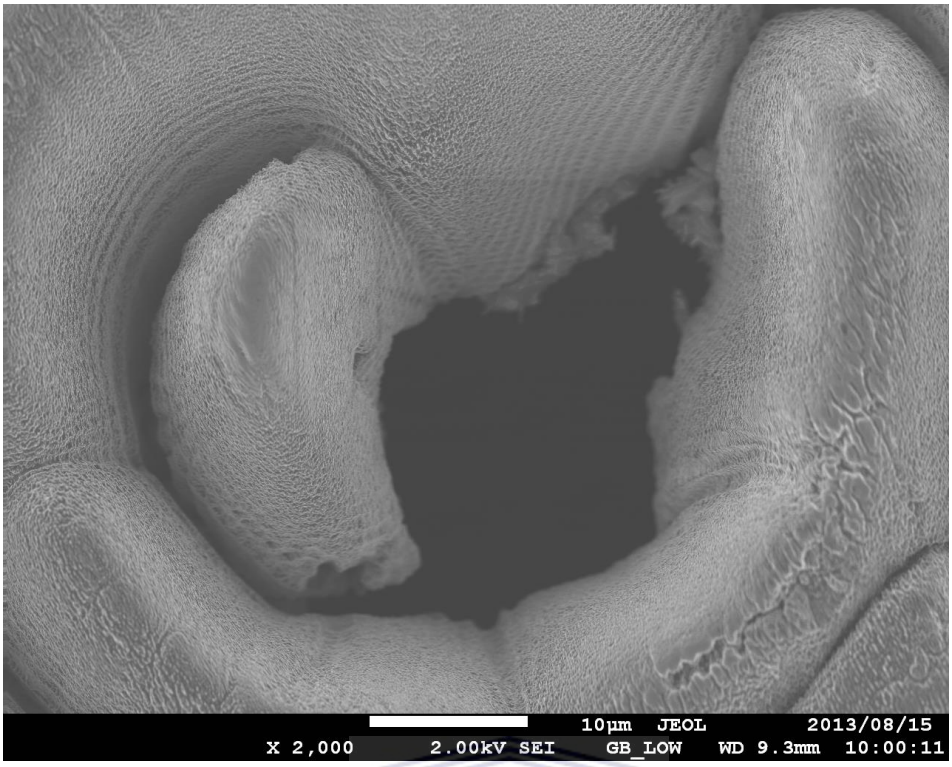

(a)

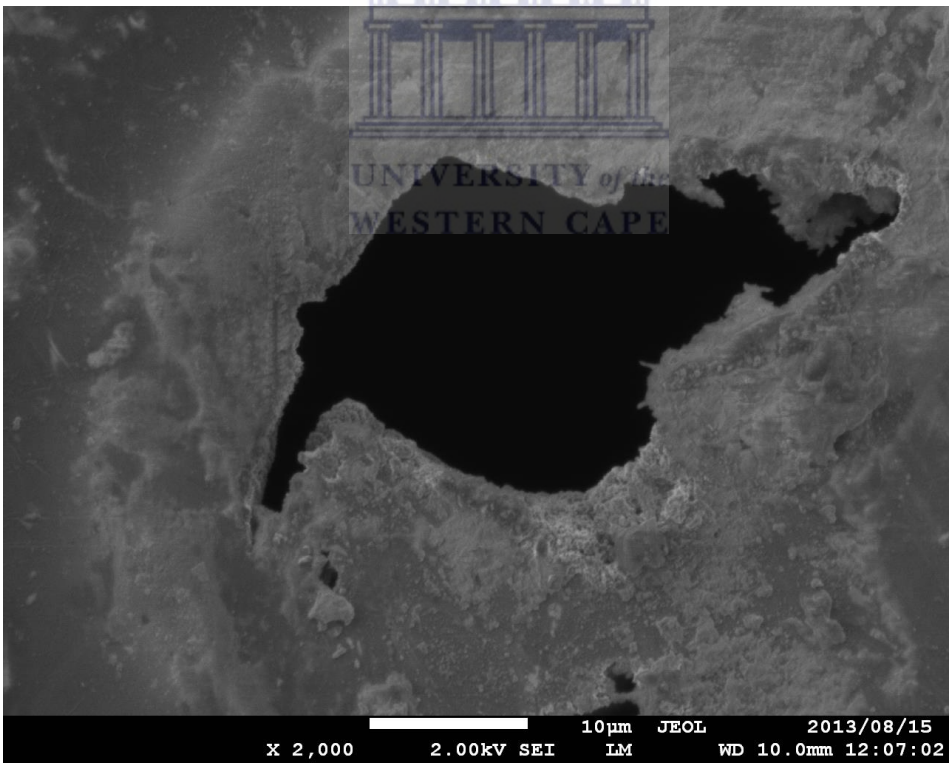

(b)

Figure 4.5: The high magnification images of the (a) entrance and (b) exit holes drilled on the 50 µm stainless steel sheet.

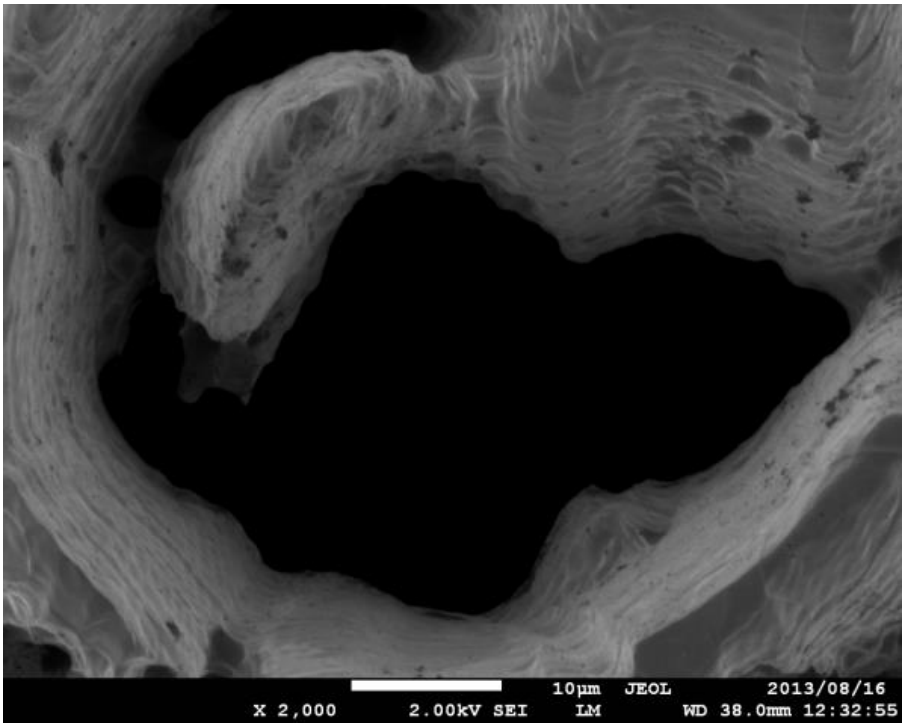

(a)

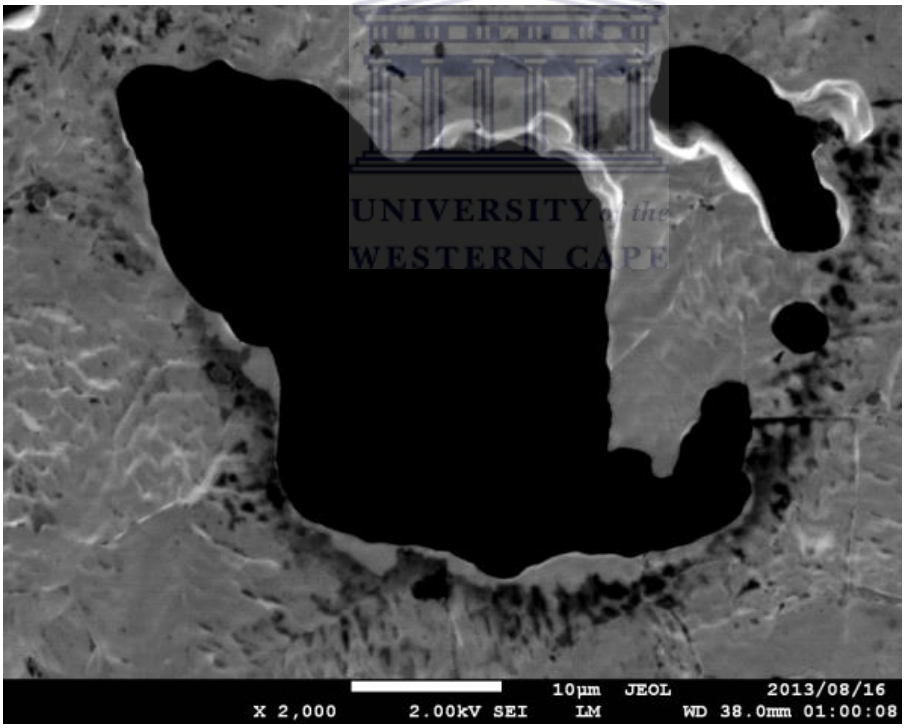

(b)

UNIVERSITY of the
WESTERN CAPE

Figure 4.6: The high magnification images of the (a) entrance and (b) exit holes drilled on the 50 µm stainless steel sheet after it was immersed in an ultrasonic bath.

(a)

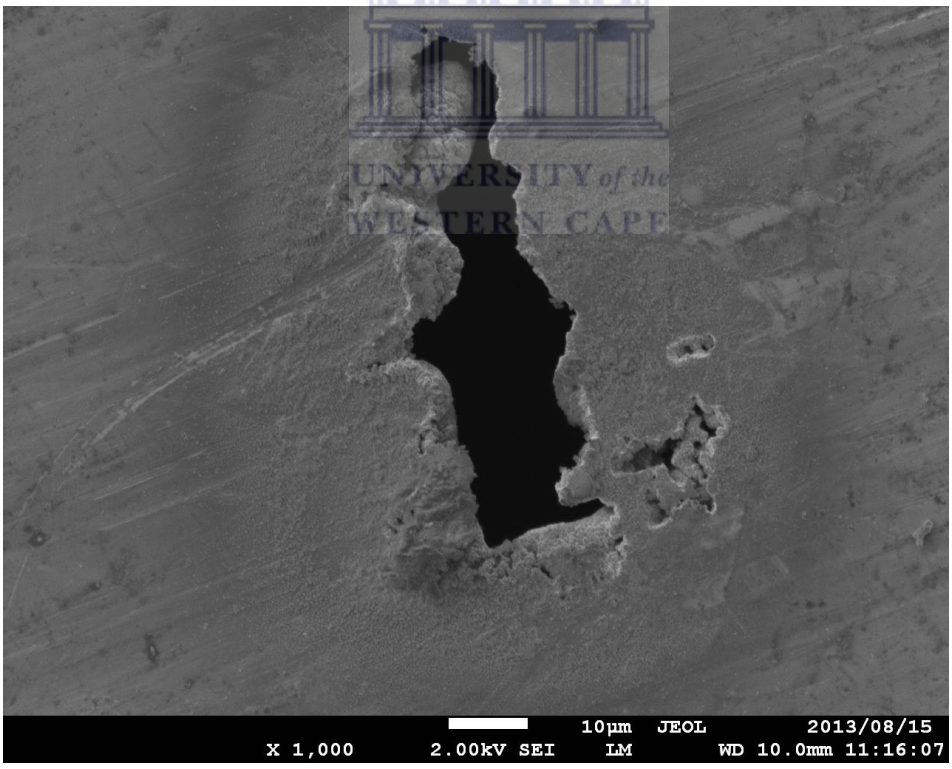

(b)

Figure 4.7: Top and bottom images of drilled stainless steel 50 µm sheet, (a) is the top surface drilled with shielding gas and (b) is its reverse side

UNIVERSITY of the
WESTERN CAPE

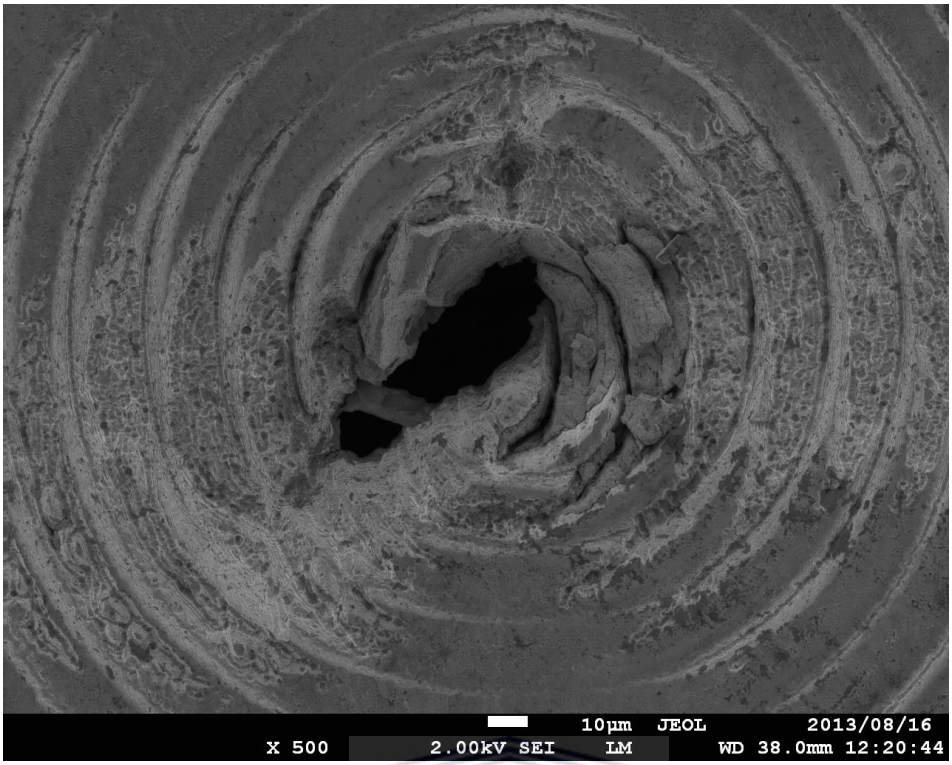

(c)

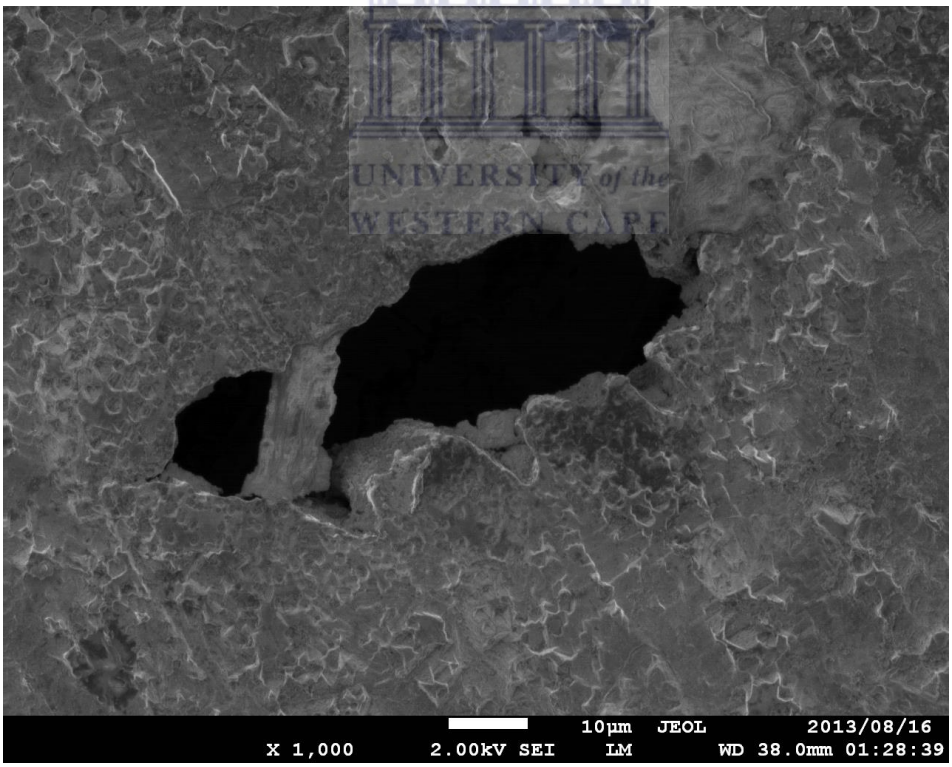

(d)

Figure 4.8: Top and bottom images of drilled stainless steel 100 µm sheet (c) is the top surface drilled with shielding gas and (d) is its reverse side.

UNIVERSITY of the
WESTERN CAPE

Evaluating images from Fig. 4.7 and Fig. 4.8 and others not shown it is observed that the holes' structure is different for each sample. This could have been caused by the difference in top surface structure per sample and also affected by the thickness of the material. Another factor that could have affected the holes deviating from being circular is the poor quality of the Bessel beam generated.

Due to the non-circularity of the drilled holes, the diameters of the drilled holes were measured at various points and in different dimensions. The holes have an elliptical shape, and this could have resulted from the un-even distribution of the intensity of the Bessel beam. The initial Gaussian beam used to illuminate the axicon is far from being a perfect Gaussian beam, it has an elliptical shape instead or a circular shape (see Fig. 3.3). As mentioned in chapter 2, a Bessel beam is formed by illuminating an axicon with a Gaussian beam, thus the quality of the Bessel beam relies on the quality of the Gaussian beam. The first surrounding rings have slightly high intensity that causes ablation on the area surrounding the central lobe; this causes the hole to be larger than the size of the central lobe of the Bessel beam.

UNIVERSITY of the
WESTERN CAPE

The stainless steel sheets were also drilled using the Gaussian beams. A lens with a focal length of 60 mm was placed in the optical path of the beam, and the sample was placed at the focal length of the lens. The holes drilled were viewed using the OM and the micrographs are shown in Fig. 4.9 and 4.10. Fig. 4.9 shows holes drilled on the 100 µm stainless steel sheet and Fig. 4.10 shows that of a 50 µm sheet.

Similarly to the holes drilled with Bessel beams, the holes drilled with Gaussian beams are also non-circular. The entrance holes have an elliptical shape that is similar to the shape of the initial Gaussian beam shown in Fig. 3.4, this is because the top surface takes on the shape of the oncoming beam. However the shape of the exit holes deviate more from being circular as the beam propagates inside the material and the original shape is lost. The exit diameters are smaller than those of the entrance holes. The shape of the holes differs for each sample, although the same setup was used. This can be attributed to the structure of the material and its positioning when drilled.

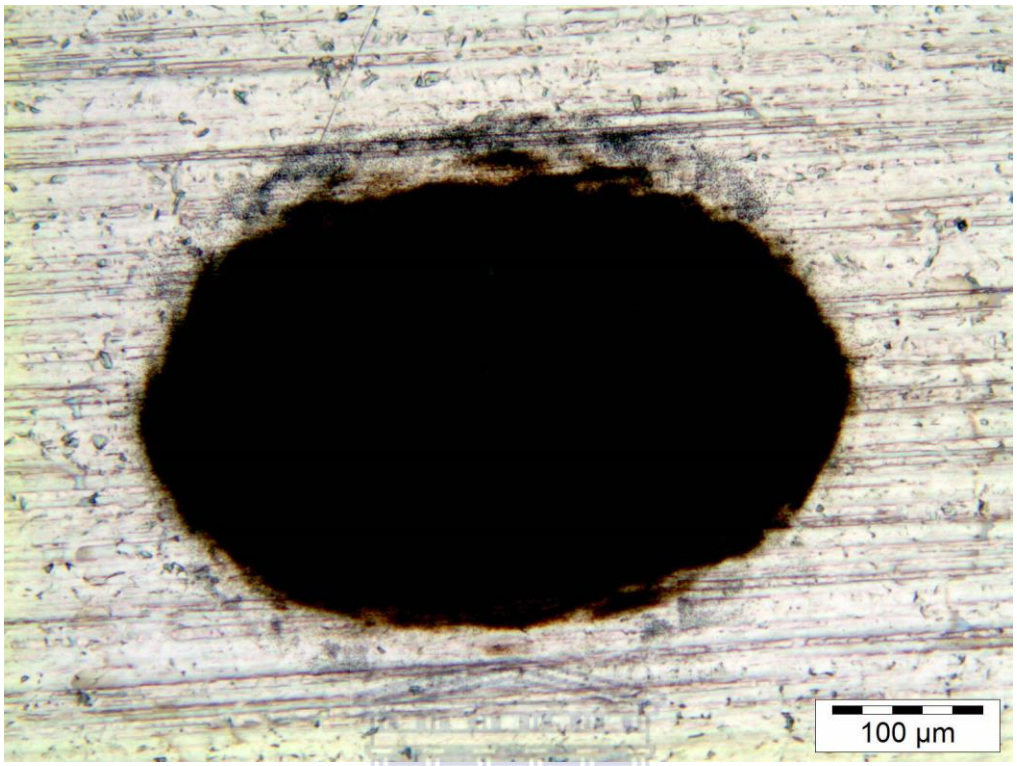

(a)

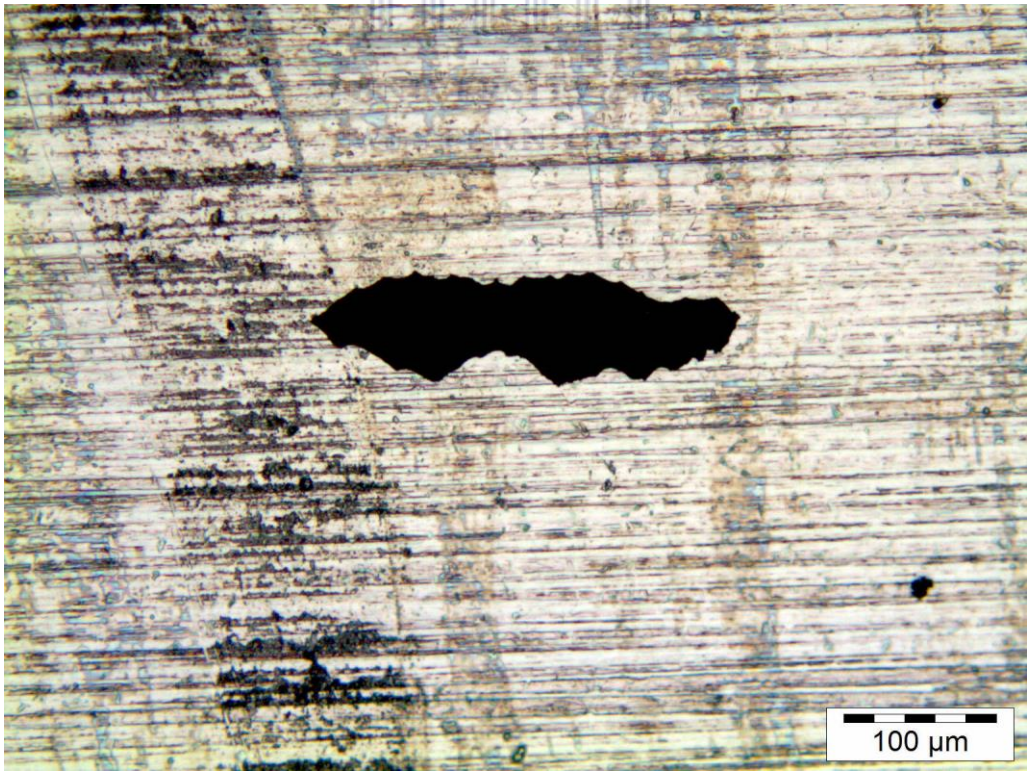

(b)

Figure 4.9: The entrance (a) and exit (b) holes drilled on a stainless steel 50 µm thick sheet using a Gaussian beam.

Figure 4.10: The entrance (a) and exit (b) holes drilled on a stainless steel 100 µm thick sheet using a Gaussian beam.

Femtosecond lasers are known to be unstable over a long period of time, thus from time to time the quality of the initial beam deteriorates. This can be seen in the difference between the beams in Fig. 2.18 (a) and Fig. 3.3. These images were taken from the same laser at different times hence their qualities differ. Every now and again the system has to be aligned to restore the beam quality. Because of this instability the shape of the drilled holes differ per sample although the setup remains the same. The elliptical shape of the initial Gaussian beam has affected the holes drilled by both Gaussian and Bessel beams.

To eliminate the problems faced above, a different choice of material was considered. From literature it has been shown that femtosecond lasers have been used successfully for fabrication of taper-free micro-channels in glass using Bessel beams [15]. As discussed in chapter 2 the Bessel beam has the ability to reconstruct itself after encountering an obstruction, this was observed when the Bessel beam passed through glass slides.

UNIVERSITY of the
WESTERN CAPE

At the operating wavelength $\lambda = 775$nm, the Bessel beam propagates through glass without being absorbed or reflected. Since the central lobe of the Bessel beam has higher intensity than the surrounding rings, it drills a hole on the 1 mm thick microscope glass slides, whilst the surrounding rings get transmitted through. The visible ring structure in Fig. 4.11 was caused by the marking that was done on the top surface of the glass specimen for ease in measuring the diameter of the hole. The diameter was measured to be 15.4 ± 0.3 µm from the OM. The hole can be clearly identified and it is more circular as compared to the holes drilled on metals above. This is because the Bessel beam reconstructs itself inside the glass slide, unlike the case of metals that are opaque.

Figure 4.11: A micrograph of a hole drilled using a Bessel beam on a painted 1 mm thick microscope glass slide.

UNIVERSITY of the
WESTERN CAPE

The measured diameter of the hole is smaller than the diameter of the central lobe of the Bessel beam, it is almost equivalent to the radius of the central lobe, $r_0 = 15.9 \pm 0.3$ µm. The hole was drilled with a femtosecond laser with a pulse energy 11.68 µJ on the central lobe. Increasing the pulse energy increases the diameter of the drilled hole, however still smaller than the diameter of the central lobe of the Bessel beam.

Through holes were drilled on the 1 mm microscopic slides as shown in Fig. 4.12. The exit diameter is smaller than the entrance diameter of the drilled hole. The entrance diameter was measured to be 16.51 µm and the exit diameter was measured to be 10.32 µm resulting in a taper angle, $\varphi = 0.18°$.

The same experiment was conducted using the same processing parameters but with two samples placed a certain distance apart. The aim of this setup was to show that Bessel beams possess a longer depth of field and its central lobe retains the same diameter along the propagation region as shown in chapter 2. Two 1 mm microscopic glass slides were placed 12 mm apart along the Bessel beam propagation zone. The Bessel beam passes through the first slide and it reconstructs itself and then passes through the second slide, producing almost the same hole. In Fig. 4.13, slide (a) was placed first followed by slide (b), and only the front surface is shown in these images for both slides. The rings surrounding the central lobe are not visible in this case, since they are of low intensity they propagate through the glass slides without causing any ablation. The holes shown in Fig. 4.13 (a) and (b) had a diameter of 20.2 ± 0.3 µm drilled with a pulse energy 14.58 µJ.

UNIVERSITY of the
WESTERN CAPE

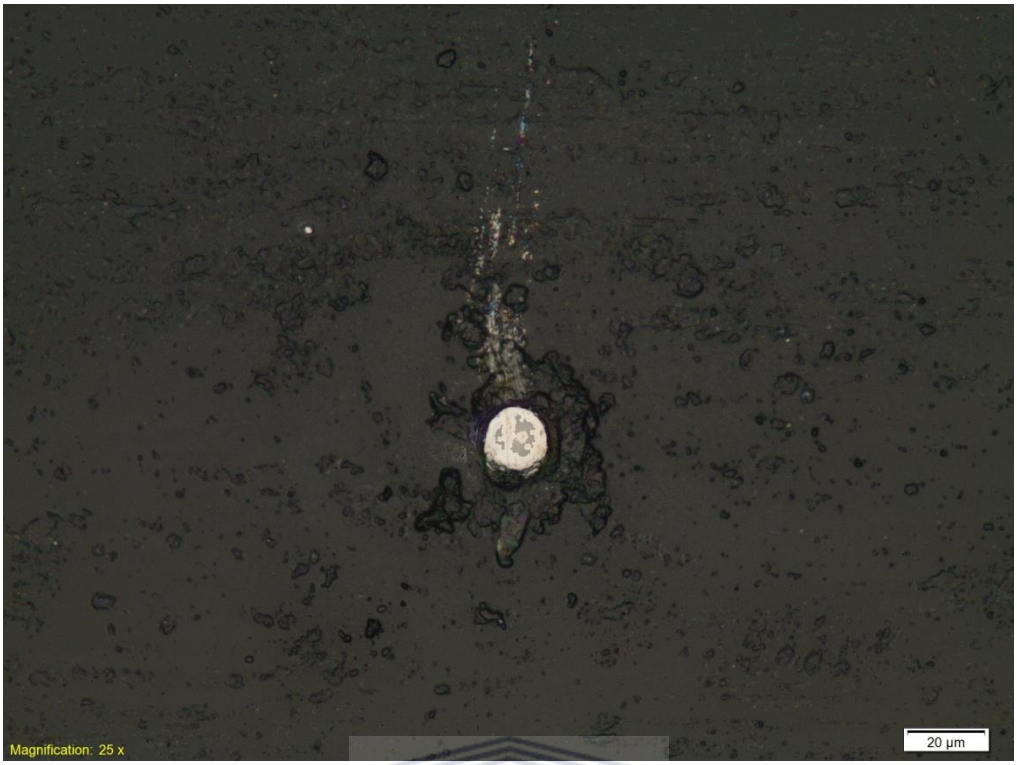

(a)

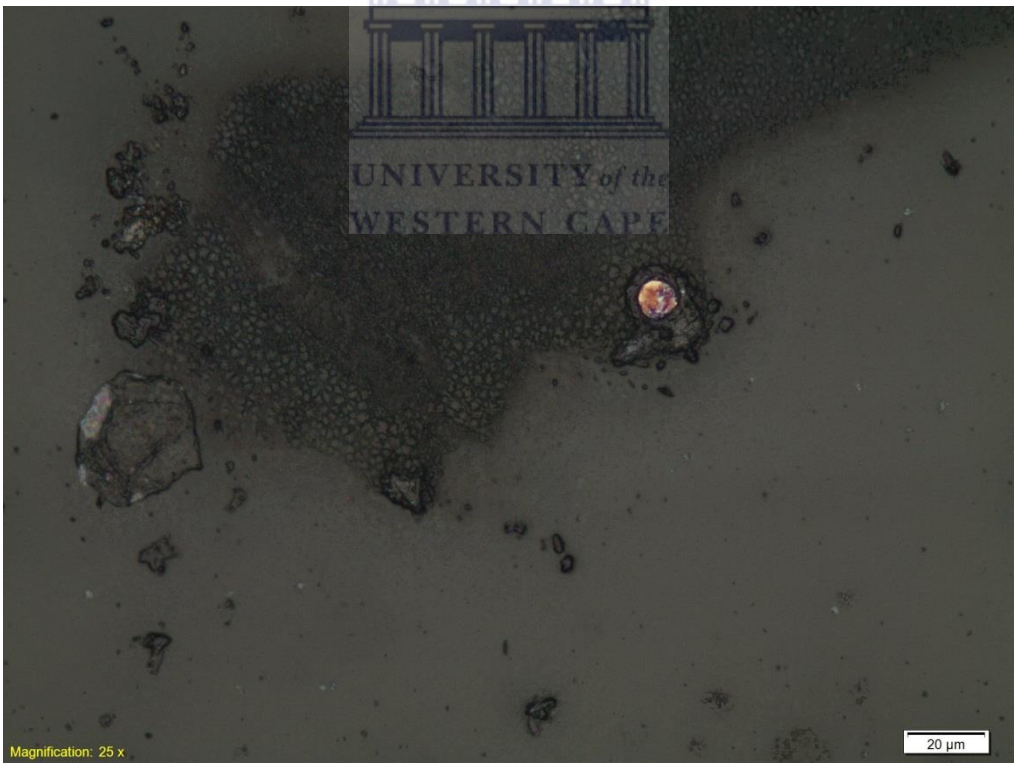

(b)

Figure 4.12: The entrance and exit diameters of holes drilled on 1 mm thick microscope glass slide.

UNIVERSITY of the
WESTERN CAPE

(a)

(b)

UNIVERSITY of the
WESTERN CAPE

Figure 4.13: Images of top surface of holes drilled on two glass samples placed a distance apart along the Bessel beam propagation zone.

Although clear holes were visible on the top surface of the glass slides, it was however difficult to view the exit holes on the bottom surface of the slides. This could be caused by the debris that can form a closure at the bottom of the hole depending on the thickness of the slides or insufficient output power from the laser. As mentioned above the femtosecond laser used in these experiments was unstable with power fluctuations. This has an effect on the overall energy distribution in the Bessel beam. When the power was low, through holes could not be drilled on the 1 mm microscope glass slides.

After the laser's output power was adjusted the above experiments we conducted again, this time around through holes were drilled on the 1 mm microscope glass slides. Figure 4.14 shows the entrance and exit diameters of the drilled holes. The measured output power was 756 mW which was enough to drill through the slides. The average entrance diameter was measured to be 16.52 µm and the exit diameter was 11.03 µm resulting in a taper angle, $\varphi = 0.14°$.

UNIVERSITY of the
WESTERN CAPE

(a)

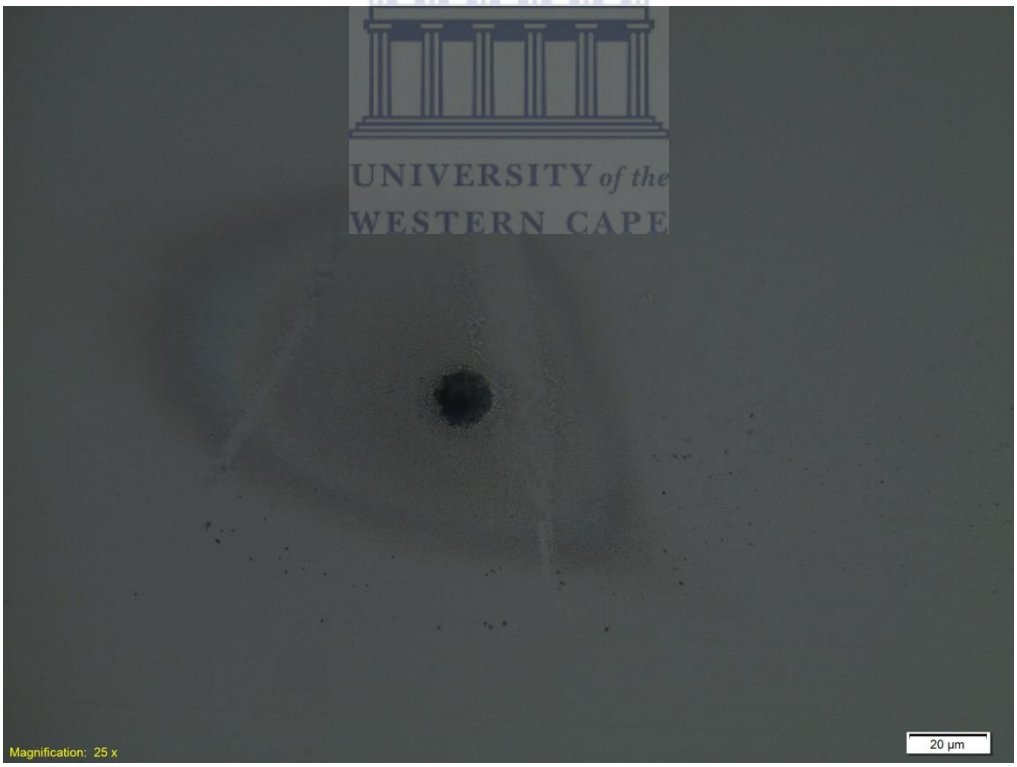

(b)

UNIVERSITY of the
WESTERN CAPE

Figure 4.14: The (a) entrance and (b) exit holes drilled on 1.1 mm microscope glass slide.

4.2 Conclusion

Laser drilling on stainless steel sheets using Bessel beams yields non-circular holes, however the entrance and exit sides contain the same shape. The intensity of the first few surrounding rings ablates the top surface of sheets causing the width of the hole to be wider than that of the central lobe of the Bessel beam. For stainless steel sheets thicker than 150 µm, through holes could not be drilled. The Bessel beam could not reconstruct itself within the metal, as the metal is opaque, hence through holes could only be drilled on very thin samples.

A different material was considered, in order to analyse the effect of using Bessel beams in microdrilling, since poor quality results were obtained using stainless steel. Microscope glass slides were then drilled using Bessel beams, and good quality holes were drilled with no visible ring structure. The diameter of the holes drilled was smaller than that of the central lobe of the Bessel beam, however increasing the pulse energy increased the diameter of the hole. The holes drilled on microscope glass slides resulted in a taper angle, $\varphi < 1°$.

The ability of Bessel beams to reconstruct after encountering an obstacle was demonstrated when two samples placed a distance apart were drilled at the same time, resulting in almost the same size holes. This also showed that the central lobe of the Bessel beam retains the same size along the propagation zone. Overall Bessel beams can be used to drill circular holes in glass with no effect of the external ring structure on the top surface of the glass sample.

The output power fluctuations affect the quality of the initial beam, which then affects the quality of the output shaped beam. When the output power is low, the pulse energy in the Bessel beam is also low, this decreases the intensity in the central lobe of a Bessel beam, resulting in drilling of vias instead of through holes.

Summary

Laser beam shaping plays a crucial role in laser drilling. In most cases laser drilling is performed using the Gaussian beam shape, however there are other beam shapes that have been alternatively used. In this dissertation the Bessel beam was used for drilling micron sized holes on different materials and its effect on the hole quality was investigated.

Zero order Bessel beams were generated using axicons and the main properties of Bessel beams, namely z_{max} and r_0 were measured. The principles that defines Bessel beams were discussed and proven experimentally. Annular beams which resulted from far fields of Bessel beams were also discussed together with means of generating them.

The generated Bessel beams were then applied in laser microdrilling processes. Stainless steel sheets ≤ 100 µm in thickness were drilled using Ti:Sapphire femtosecond lasers. Since metals are opaque one of the special properties of Bessel beams was not met. The principle of reconstruction of a Bessel beam after encountering an obstacle was not possible for the stainless steel sheet, since the beam could not propagate through the sheets. The holes drilled on stainless steel sheets were not circular but however they maintained the same shape at the top and rear surface of the samples. This showed that Bessel beams can drill parallel holes with minimal taper on materials.

Bessel beams proved to have better drilling effects on glass materials than on metals. Well defined circular holes were drilled on transparent 1 mm thick microscope glass slides.

UNIVERSITY of the
WESTERN CAPE

Future work

For future work, a laser with a good beam quality, M^2, should be used to generate good quality Bessel beams. This could help improve on the circularity of the drilled beams.

The possibility of drilling through holes on transparent glass materials could be further investigated, with focus on the microstructure of the hole created. The main idea will be to investigate the propagation of the intensity distribution from the central spot size of the Bessel beam within the walls of the drilled hole.

UNIVERSITY of the
WESTERN CAPE

References

1. Y. Matsuoka, Y. Kizuka, and T. Inoue, 'The characteristics of laser micro-drilling using a Bessel beam', J. Appl. Phys. **A 84**, (2006) 423.
2. M. Kohno, and Y. Matsuoka, 'Microfabrication and drilling using diffraction-free pulsed laser beam generated with axicon lens.' JSME International Journal Series **B 47** (3), (2004) 497.
3. K. Walther, M. Brajdic, and W. Wawers, Drilling. In: R. Poprawe (ed.), *Tailored Light 2 Laser Application Technology*. RWTH edition, Berlin Heidelberg: Springer, (2011) 365.
4. A. G. Corfe and R. C. Crafer, Drilling. In: D. Schuöcker (ed.), *Handbook of the EuroLaser Academy*, Volume 2, London: Chapman & Hall, (1998) 523.
5. N.B. Dahotre and S.P. Harimkar, *Laser Fabrication and Machining of Materials*, Springer, (2008) 97.
6. S. Bandyopadhyay, J. K. Sarin Sundar, G. Sundararajan, S. V. Joshi, 'Geometrical features and metallurgical characteristics of Nd:YAG laser drilled holes in thick IN718 and Ti-6Al-4V sheets'. Journal of Materials Processing Technology **127**, (2002) 83.
7. M. Duocastella and C. B Arnold, 'Bessel and annular beams for materials processing'. Laser & Photonics Rev. **6** (5), (2012) 607.
8. N. Sanner, N. Hout, E. Audouard, C. Larat and J.P Huignard, 'Direct ultrafast laser micro-structuring of materials using programmable beam shaping,' Opt. Laser Eng. **45** (6), (2007) 737.
9. J. Durnin, J. J. Miceli Jr., and J. H. Erbely, 'Diffraction-free beams,' Phys. Rev. Lett. **58**, (1987) 1499.
10. J. Durnin, 'Exact solutions for nondiffracting beams. I. The scalar theory,' J. Opt. Soc. Am. **A 4** (1987) 651.
11. I. A. Litvin, M. G. McLaren and A. Forbes, 'A conical wave approach to calculating Bessel-Gauss beam reconstruction after complex obstacles,' Opt. Commun. **282** (6), (2008) 1078.
12. M. G. McLaren, Optical tweezing and micromanipulation, MSc Thesis University of Witwatersrand, (2009).
13. R. Paschotta, Encyclopaedia of Laser Physics and Technology, RP Photonics Consulting, Wiley VCH, www.rp-photonics.com. Last accessed 22-03-2013.

UNIVERSITY of the
WESTERN CAPE

14. B. E. A. Saleh and M. C. Teich. *Fundamentals of Photonics*. John Wiley & Sons, Inc., Hoboken, New Jersey, 2007.
15. I. A. Litvin, M. G McLaren, and A. Forbes, 'Propagation of obstructed Bessel and Bessel-Gauss beams,' SPIE **7062** (706218), (2008) 1.
16. J. Arlt and K. Dholakia, 'Generation of higher-order Bessel beams by use of an axicon,' Opt. Commun. **177,** (2000) 297.
17. D. McGloin and K. Dholakia, 'Bessel beams: diffraction in a new light,' Contemporary Physics **46** (1), (2005) 15.
18. R. Vasilyeu, A. Dudley, N. Khilo, and A. Forbes, 2009, 'Generating superpositions of higher-order Bessel beams,' Opt. Express **26** (17) (2009) 23389.
19. Y. Ismail, N. Khilo, V. Belyi, and A. Forbes, 'Shape invariant higher-order Bessel-like beams carrying orbital angular momentum,' J. Opt. **14** (8), (2012) .
20. M. Mazilu, D. J. Stevenson, F. Gunn-Moore and K. Dholakia, 'Light beats the spread: "non-diffracting" beams,' Laser Photonics Rev. **4** (4) (2010), 529.
21. C. A. McQueen, J. Arlt, and K. Dholakia, 'An experiment to study a "nondiffracting" light beam,' Am. J. Phys. **67**, (10) (1999) 912.
22. K. H. Alexeev, A. Leitz, Otto, and M. Schmidt, Applications of Bessel beams for ultrafast laser volume structuring of non-transparent media, Phys. Proc. **5**, (2010) 533.
23. F. Courvoisier, M. K. Bhuyan, P. A. Lacourt, M. Jacquot, L. Furfaro, and J. M Dudley, 'Material Nanoprocessing with Nondiffracting Femtosecond Bessel beams,' IEEE, ISBN 978-1-4244-7797 (2010) 1.
24. J. H. McLeod, 'The axicon: a new type of optical element,' J. Opt. Soc. Am **44**, (1954) 592.
25. http://www.thorlabs.com. Last accessed 02-04-2013
26. P. Fischer, H. Little, R. L. Smith, C. Lopez-Mariscal, C. T. A. Brown, W. Sibbet, and K. Dholakia, 'Wavelength dependent propagation and reconstruction of white Bessel beams,' J. Opt. A. Pure Appl. Opt **8**, (2006) 477.
27. M. K. Bhuyan, F. Courvoisier, P. A Lacourt, M. Jacquot, L. Furfaro, M. J. Withford, and J. M. Dudley, 'High aspect ratio taper-free microchannel fabrication using femtosecond Bessel beams,' Opt. Exp. **18** (1), (2010) 566.

UNIVERSITY of the
WESTERN CAPE

28. R. Inoue, K. Takakusaki, Y. Takagi, and T. Yagi, 'Micro-ablation on silicon by femtosecond laser pulses focused with an axicon assisted with a lens,' Appl. Surf. Sci. **257**, (2010) 476.
29. B. N. Chichkov, C. Momma, S. Nolte, F. Von Alvensleben, and A. Tunnermann, 'Femtosecond, picosecond and nanosecond laser ablation of solids,' Appl. Phys. A. **63** (1996) 109.
30. V. Zambon, N. McCarthy, and M. Piché, 'Fabrication of Photonics Devices Directly Written in Glass Using Ultrafast Bessel Beams,' SPIE **7099** (70992J), (2008) 1.
31. V. Zambon, N. McCarthy, and M. Piché, 'Laser Micromachining of Transparent Glass Using Ultrafast Bessel Beams,' SPIE. **7386** (738632), (2009) 1.
32. W. K. Fester, M. Abramowitz, I. D. Johnson, R. T. Sutter, M. J. Parry-Hill, M.W.Davidson.http://www.olympusmicro.com/primer/java/infinityoptics/magnification/index.html. Last accessed 04-04-2013
33. M. R. H Knowles, G. Rutterford, D. Karnakis, and A. Ferguson, 'Micro-machining of Metals, Ceramics and Polymers using Nanosecond Lasers,' Int. J. Adv. Manuf. Technol **33**, (2007) 95.
34. S. Dhar, N. Saini, and R. Purohit, 'A review on laser drilling and its techniques,' International Conference on Advances in Mechanical Engineering (2006), December 1-3.
35. E. Kannatey-Asibu Jr., *Principles of Laser Materials Processing*, Hoboken, New Jersey, Wiley (2009) 467.
36. G. K. L. Ng and L. Li, 'Repeatability characteristics of laser percussion drilling of stainless-steel sheets,' Optics and Lasers in Engineering, **39**, (2003) 25.
37. E. Kacar, M. Mutlu, E. Akman, A. Demir, L. Candan, T. Canel, V. Gunay, T. Sinmazcelik, Characterization of the drilling alumina ceramic using Nd:YAG,' Journal of Materials Processing Technology **209**, (2009) 2008.
38. B. S. Yilbas and A. Aleem, 'Laser hole drilling quality and efficiency assessment,' Proc. Instn Mech. Engrs, Part B: Journal of Engineering Manufacture **218**, (2004) 225.
39. R. Paschotta, Encyclopaedia of Laser Physics and Technology, RP Photonics Consulting, Wiley VCH, www.rp-photonics.com. Last update 22-03-2013.

UNIVERSITY of the
WESTERN CAPE

40. P. Baricholo, J. Steyn, A. Du Plessis, T. Roberts, L. Botha, H. M. von Bergmann, 'Ultrafast laser microhole drilling of medical catheter material, thin ceramic and stainless steel plates,' (2004) 1.
41. C. A. Biffi, N. Lecis, B. Previtali, M. Vedani, G. M. Vimercati, 'Fiber laser microdrilling of titanium and its effect on material microstructure,' Int. J Adv. Manuf. Technol **54**, (2010) 149.
42. J Rockstroh, X. Chen, W. T. Loshaw, 'Influence of laser pulse duration on laser drilled hole quality in nickel based super alloy,' ICALEO C, (1996), 113.
43. C. Y. Yeo, The Physics of laser processing, J Matter Process, Technol. **42**, (1994) 15.
44. F. Courvoisier, P. A. Lacourt, M. Jacquot, M. K. Bhuyan, L. Furfaro, and J. M. Dudley, 'Surface nanoprocessing with nondiffracting femtosecond Bessel beams,' Optics letters, **34**, (20) (2009) .
45. M. D. Perry, B. C. Stuart, P. S. Banks, M. D. Feit, V. Yanovsky and A. M. Rubenchik, 'Ultrashort-pulse laser machining of dielectric materials,' J. Appl. Phys. **85** (9), (1999) 6803.
46. Optical Microscope. Available at: en.wikipedia.org/wiki/Optical-microscope, last accessed: 20-08-2013
47. http://www.freeinfosociety.com, last accessed: 20-08-2013
48. J. Goldstein, *Scanning Electron Microscopy and X-ray Microanalysis*, Third Edition, Springer, 2003.
49. http://cmrf.research.uiowa.edu/scanning-electron-microscopy, last accessed 22-08-2013
50. D. Chescoe and P. J. Goodhew, '*The Operation of Transmission and Scanning Electron Microscopes*, 1990.
51. P. J. Goodhew and F. J. Humphreys, *Electron Microscopy and Analysis*, 2nd Edition, Taylor & Francis, London, 1988.

UNIVERSITY of the
WESTERN CAPE